ACS OMEGA

Open Access

http://pubs.acs.org/journal/acsodf

Article

Effect of Microfluidization on the Volatiles and Antibacterial, Antifungal, and Cytotoxic Activities of Algerian *Satureja hortensis* L. Oil-Loaded Nanoemulsions: *In Vitro* and *In Silico* Study

Amel Boudechicha, Abdelhakim Aouf, Hatem Ali, Tawfiq Alsulami, Ahmed Noah Badr, Zhaojun Ban, and Amr Farouk*

Cite This: *ACS Omega* 2024, 9, 27030−27046

Read Online

ACCESS | Metrics & More | Article Recommendations | Supporting Information

ABSTRACT: This study aimed to increase the stability and solubility of the Algerian *Satureja hortensis* L. (ASHO) essential oil through nanoencapsulation. Nanoemulsions of ASHO (MF-ASHEO) were developed to evaluate their antioxidant and antimicrobial potential, stability, and cytotoxicity using microfluidization at 150 MPa for five cycles. MF-ASHO showed 8 compounds (99.56%) vs ASHEO's 26 compounds (95.46%). Carvacrol increased to 94.51%, replacing γ-terpinene, which decreased to 0.43%. The MF-ASHEO nanoemulsion had a mean particle size of 41.72 nm, a monomodal size distribution pattern, a mean ζ-potential of −39.4 mV, and a polydispersity index (PDI) mean value of 0.291. Micrographs showed spherical nanoparticles with varying diameters in nm. ASHEO was more toxic than MF-ASHEO against HepG2, Vero, and WI-38, according to the MTT and WST-1 assays. ASHEO demonstrated antiradical and antibacterial activity and inhibited biofilm formation. It also had an enhanced antifungal effect and reduced mycotoxin production. The MF-ASHEO sample showed no activity except in reducing mycotoxin production, where it performed better than ASHEO. *In silico* and ADME results confirmed the inhibitory action of carvacrol on the key enzymes of the aflatoxin biosynthetic mechanism and the target proteins associated with bactericidal/bacteriostatic effects. The microfluidization process dramatically affects not only the oil's volatile content but also its biological activity.

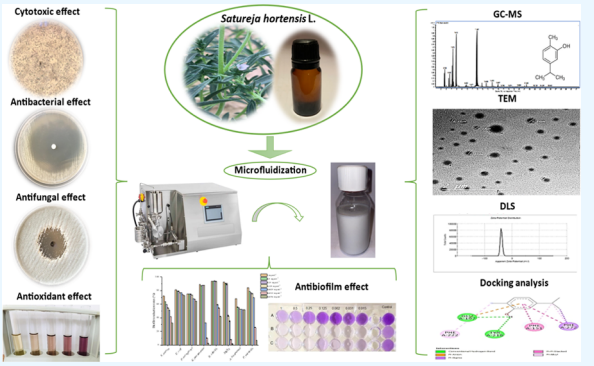

1. INTRODUCTION

Plants from families such as *Boraginaceae*, *Lamiaceae*, and *Solanaceae* are cultivated worldwide for their bioactive constituents, such as essential oils, alkaloids, and polyphenols. These oils are natural protectants against predators and environmental stressors and are now commonly used daily.[1] Summer savory (*Satureja hortensis* L.) is a Mediterranean herb with linear leaves from the *Lamiaceae* family. It is used in cooking and medicine. Extracts and oils from the herb contain compounds that can prevent diabetes, cardiovascular diseases, and cancer and provide antioxidant, antimicrobial, and anti-inflammatory benefits.[2]

According to the literature, the essential oil of *S. hortensis* contains α-pinene, β-pinene, p-cymene, γ-terpinene, α-terpinolene, α-thujene, carvacrol, thymol, and caryophyllene, which have antibacterial, antiviral, and antifungal effects.[3,4] The variation in results obtained by different authors is due to factors such as season, climate, and genetics.[5] Therefore, the source and composition should be clearly stated when discussing the potential use of essential oils or extracts from summer savory. For example, the essential oil obtained from Bordj-Ménaïel, 65 km North of Algiers, is characterized by carvacrol and γ-terpinene,[6] while the oil collected from jedioua Relizane situated in the North West of Algeria was characterized by cadinol, thymol, himachalene, and selinene.[7] No data are available concerning the *S. hortensis* essential oil from Bou Saada, M'Sila Province, to the South of Algiers.

Essential oil from *S. hortensis* is used in various industries, such as the food industry and aromatherapy,[4] but treatments and heating processes can alter its composition and thermal properties. To avoid such drawbacks, encapsulating essential oils through nanoemulsions in delivery systems can optimize solubility and stability and improve reactivity, absorption, and controlled release, extending their applications in the food and pharmaceutical industries.[8] Microfluidization is a high-energy technique that has successfully produced nanoemulsions with sizes below 200 nm, such as in lemongrass.[8] This method involves pumping a coarse emulsion under high pressure

Received: January 9, 2024
Revised: May 25, 2024
Accepted: May 31, 2024
Published: June 11, 2024

Table 1. Percentage of Volatile Components of ASHEO and MF-ASHEO Identified by GC-MS Analysis

S/N	compound	RI[a]	LRI[b]	area%		identification method[c]
				ASHEO	MF-ASHEO	
1	α-thujene	933	930	2.30		RI, MS, STD
2	α-pinene	942	939	2.74		RI, MS, STD
3	camphene	955	954	0.29		RI, MS
4	β-pinene	981	979	1.64		RI, MS, STD
5	β-myrcene	993	990	2.54		RI, MS, STD
6	α-phellandrene	1004	1002	0.50		RI, MS
7	α-terpinene	1018	1017	3.38		RI, MS, STD
8	p-cymene	1023	1024	9.01		RI, MS, STD
9	limonene	1031	1029	1.19		RI, MS, STD
10	E-β-ocimene	1049	1050	0.22		RI, MS
11	γ-terpinene	1061	1059	17.72	0.43	RI, MS, STD
12	cis-sabinene hydrate	1073	1070	0.18		RI, MS
13	terpinolene	1092	1088	0.27		RI, MS
14	borneol	1170	1169	0.92		RI, MS
15	terpinen-4-ol	1181	1177	0.93	0.51	RI, MS
16	isothymol methyl ether	1240	1244	0.19		RI, MS
17	bornyl acetate	1285	1288	-	0.44	
18	thymol	1289	1290	2.16	1.48	RI, MS, STD
19	carvacrol	1299	1298	45.15	94.51	RI, MS, STD
20	carvacryl acetate	1337	1340	1.14	0.87	RI, MS
21	β-cubebene	1390	1388	0.20		RI, MS
22	β-caryophyllene	1415	1419	0.80		RI, MS
23	aromadendrene	1440	1439	0.28		RI, MS
24	β-bisabolene	1507	1505	1.32		RI, MS
25	spathulenol	1577	1578	0.39		RI, MS
26	caryophyllene oxide	1584	1582	1.30	0.82	RI, MS
27	α-cadinol	1655	1654	0.95	0.50	RI, MS
	total	-	-	95.46	99.56	-

[a]RI: Retention indices calculated on the DB-5 column using alkane standards. [b]LRI: Retention indices according to the literature. [c]Confirmed by comparison with the retention indices, the mass spectrum of the authentic compounds, and the NIST mass spectrum library data. ASHEO: Algerian *S. hortensis* L. essential oil and MF-ASHEO: microfluidizing emulsion of Algerian *S. hortensis* L. essential oil.

through an interaction chamber with two flow channels, which may affect the oil's volatile profile qualitatively and quantitatively. Carvacrol is the principal constituent in *S. hortensis* oil as well as the primary compound in thyme, oregano, pepperwort, and wild bergamot essential oils. It has antioxidant, antimicrobial, and antiparasitic properties and anti-inflammatory, antinociceptive, hepatoprotective, anticancer, antitoxigenic fungal, and pain management activity.[9,10] The study by Mohtashami et al.[11] demonstrated that the quality of *S. hortensis* oil improves with storage due to increased carvacrol content from 50.69 to 57.66%. Meanwhile, heating treatment at 190 °C for 2.5 h increases the concentration of carvacrol to more than 91%, which is a quick way to extract carvacrol from the essential oil, making it a suitable natural preservative for the food industry and alternative medicine.[4] However, the impact of high-pressure homogenization techniques on the carvacrol content of *S. hortensis* oil in nanoemulsion formulation, specifically microfluidization, has yet to be published.

Consequently, this study aimed to find the correlation of high-pressure homogenization (HPH) using the microfluidization technique with the chemical composition of Algerian *S. hortensis* essential oil (ASHEO) during nanoemulsion formulation, a novel approach in the field. Due to the increasing use of natural extracts like essential oils in nanoemulsion forms, it is necessary to study their biological activities to ensure the effectiveness and quality of products. Thus, this study also evaluated the microfluidization effect on *in vitro* antioxidant, antimicrobial, antibiofilm, and antiaflatoxin properties. Additionally, complementary to the *in vitro* biological examinations of the oil and its nanoemulsion, the molecular docking of carvacrol was performed with aflatoxin biosynthesis enzymes and target proteins associated with bactericidal/bacteriostatic effects, such as DHPS, DHFR, Ddl, penicillin-binding protein 1a (PBP1a), DNA gyrase, type-IV topoisomerase, and isoleucyl-tRNA synthetase (IARS), to elucidate and identify a possible mechanism of action correlated with the recorded antimicrobial or antiaflatoxin effects. The ADME profile and druglikeness properties of carvacrol were also assessed to establish its efficiency and drug ability.

2. RESULTS

2.1. Effect of the Microfluidization Technique on ASHEO Volatiles. In this study, the oil was extracted from Algerian *S. hortensis* L. using hydrodistillation. The extraction yield was 2.78% (w/v). Carvacrol (45.15%) and γ-terpinene (17.72%) were the most abundant compounds found in ASHEO (Table 1 and Figure 1A). Nanoemulsion formulation by microfluidization (MF-ASHEO) resulted in a significant increase in the carvacrol content (94.51%) at the expense of γ-terpinene (0.43%) and p-cymene (not detected) compared to the control sample (ASHEO) as shown in Table 1 and Figure 1B. The Supporting Information presents complete data in Figures S1 (oil) and S2 (MF nanoemulsion).

https://doi.org/10.1021/acsomega.4c00315
ACS Omega 2024, 9, 27030−27046

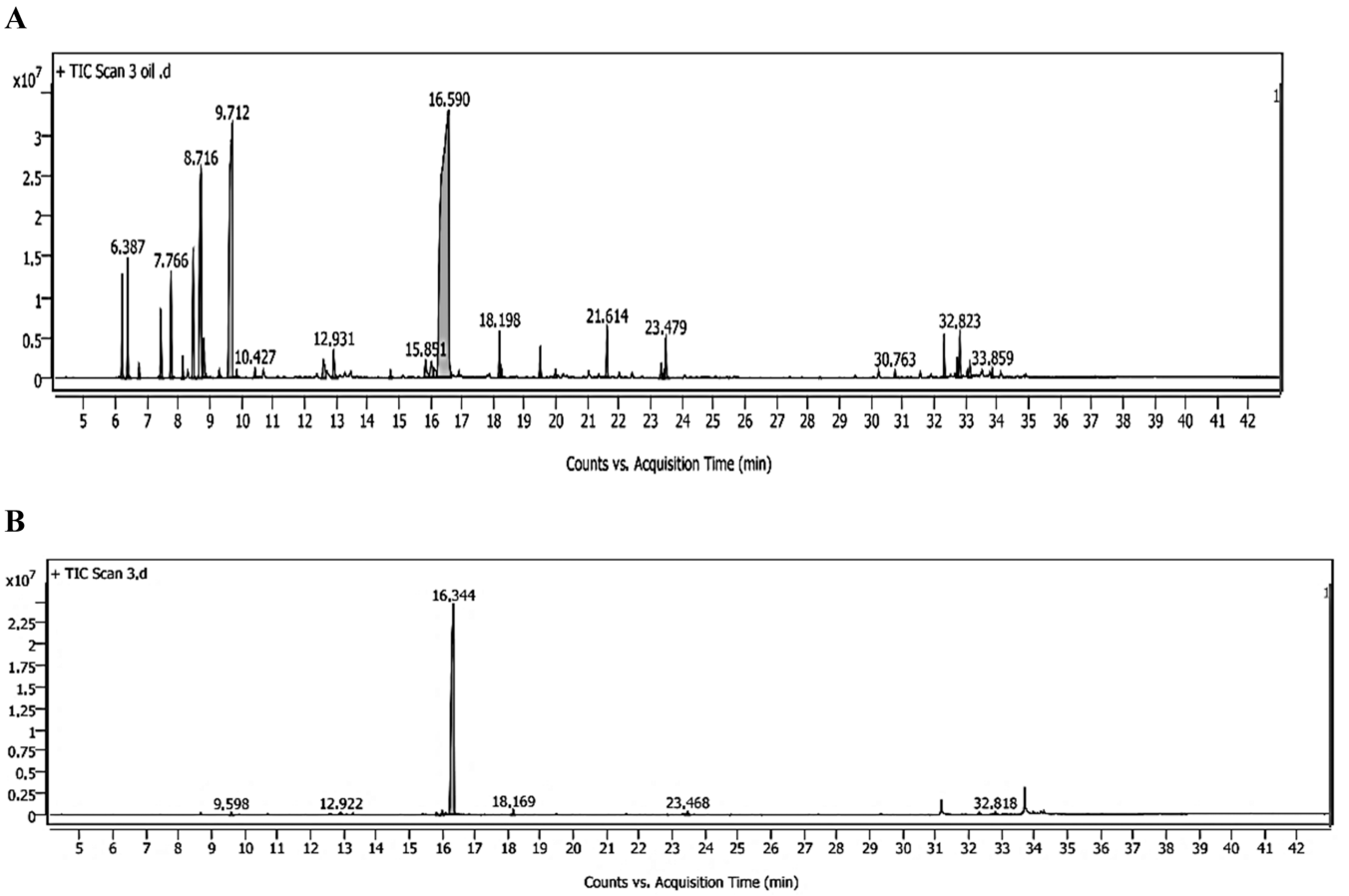

Figure 1. Volatile chromatograms for (A) ASHEO and (B) MF-ASHEO.

2.2. Characterization of the Nanoparticles. Physical characterizations of the microfluidic nanoemulsion are shown in Table 2. Samples gave an average value of 100% height ratio, indicating high stability with no observed phase separation, creaming, or sedimentation.

Table 2. Physical Characterizations of the Microfluidic Nanoemulsion[a]

property	value
refractive index	1.34 ± 0.05
density (g/mL)	0.98 ± 0.001
pH	6.22 ± 0.004
stability (separation in mm)	ND*

[a]• ND: not detected.

The MF-ASHEO nanoemulsion has a mean particle size of 41.72 ± 12.72 nm with a monomodal size distribution pattern, demonstrating ultrafine size as it was less than 100 nm and a mean ζ-potential of −39.4 ± 3.75 mV (Figure 2A,B). The polydispersity index (PDI) has dispersions' uniformity with a mean value of 0.291 ± 0.04.

The transmission electronn microscopy (TEM) characterization of the MF-ASHEO nanoemulsion showed that the droplets were evenly distributed and appeared black, indicating successful preparation. TEM micrographs revealed spherical nanoparticles with varying diameters in nanometers (Figure 3A,B).

2.3. Cytotoxic Activity. This study aimed to analyze the impact of ASHEO and MF-ASHEO on the cytotoxicity of HepG2, Vero, and WI-38 cells using MTT and WST-1 viability assays, with cisplatin as the reference drug. The results indicated that both ASHEO and its nanoemulsions significantly decreased the cell viability of HepG2 cells compared with Vero and WI-38 cells. The oil demonstrated the most potent growth inhibitory activity against the HepG2 cell line, with the lowest IC_{50} (16.69 and 23.92 μg/mL) compared to cisplatin (IC_{50} 20.71 and 40.95 μg/mL) in both MTT and WST-1 assays, respectively. The lower IC_{50} values of HepG2 cells than those of the Vero and WI-38 cell lines indicate the selectivity of ASHEO and its microfluidized nanoemulsion, as shown in Table 3.

In Figure 4, the cell morphology of HepG2 exposed to ASHEO and MF-ASHEO was observed at concentrations of 15.62 and 125 μg/mL for 24 h compared to the control cell line. These concentrations were selected as they demonstrated cell viability below 50% *via* the MTT assay. The findings showed that the changes in HepG2 cell lines were concentration-dependent. The cells exposed to ASHEO and MF-ASHEO demonstrated significant morphological alterations with a lower cell count per field, indicating cell release during exposure. This suggests that ASHEO and MF-ASHEO may substantially affect cell membranes. Additionally, a large formation of lipid vacuoles in the cells was observed. The HepG2 cells underwent morphological changes, appearing shrunken and smaller with enlarged gaps between cells and an irregular, rounded shape compared to the control group. Furthermore, some cells shrank at concentrations below the

https://doi.org/10.1021/acsomega.4c00315
ACS Omega 2024, 9, 27030−27046

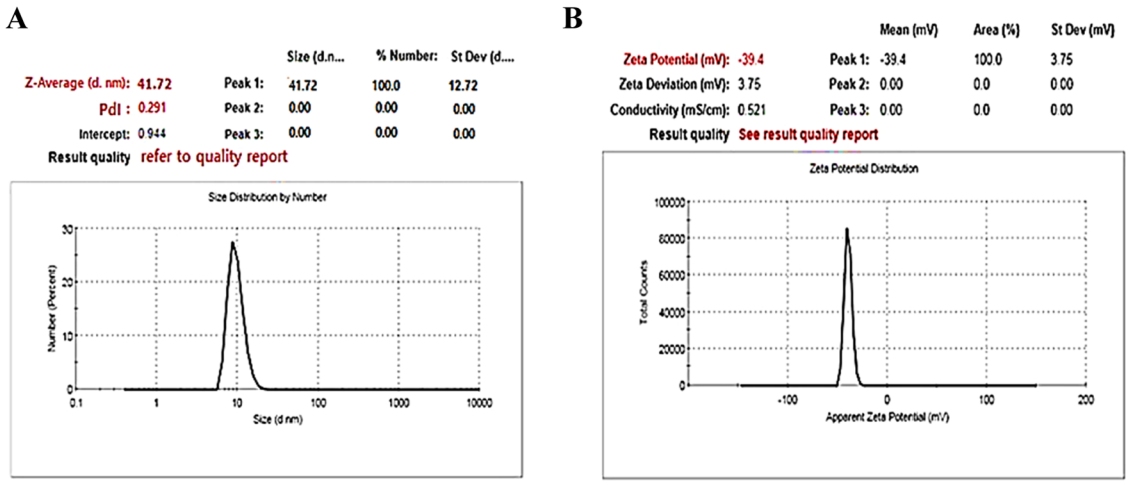

Figure 2. (A) Particle size distribution and (B) ζ-potential of the MF-ASHEO nanoemulsion.

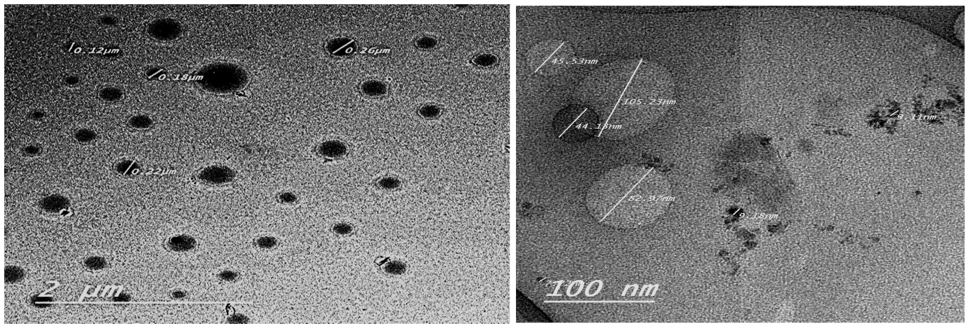

Figure 3. TEM micrograph of the MF-ASHEO nanoemulsion.

Table 3. Cytotoxic Assessment of ASHEO and Its Microfluidized Nanoemulsion against HepG2, Vero, and WI-38 Cell Lines Using MTT and WST-1 Assays

	ASHEO (IC_{50} µg/mL)		nanoemulsion (IC_{50} µg/mL)		cisplatin (control) (IC_{50} µg/mL)	
cell line	MTT	WST-1	MTT	WST-1	MTT	WST-1
HepG2	16.69 ± 0.5[a]	23.92 ± 2.0	126.0 ± 1.82	249.08 ± 2.77	20.71 ± 1.15	40.95 ± 1.88
Vero	88.34 ± 5.0	89.94 ± 4.91			142.33 ± 4.12	287.6 ± 3.43
WI-38			207.15 ± 2.61	648.71 ± 4.11	277.6 ± 4.5	401.2 ± 3.66

[a]The data were expressed as means ± SEM (where $n = 3$, $p \leq 0.05$); SD: standard division.

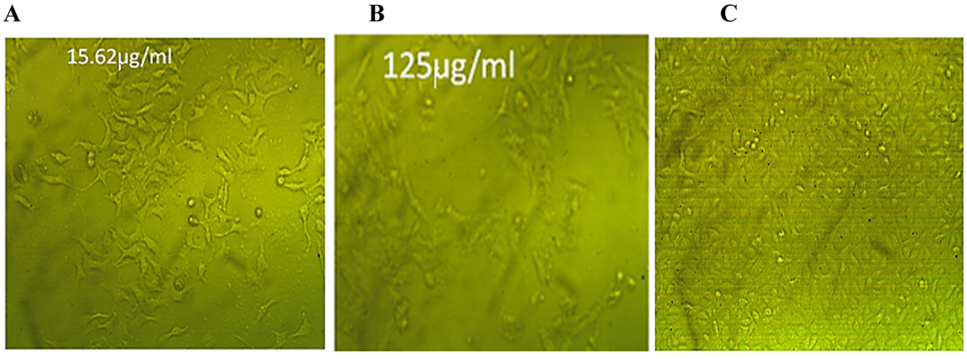

Figure 4. Morphology of HepG2 cells after cultivation for 24 h with the treatments at (A) ASHEO and (B) MF-ASHEO compared to (C) control cell line.

IC_{50} and developed a torn membrane, indicating apoptotic cell death.

2.4. Antibacterial Activity. *2.4.1. Agar Diffusion.* The antibacterial activity was assessed using a disc diffusion method. The results showed the potent activity and large spectra of ASHEO. This essential oil was active on all tested strains, with inhibition zones ranging between 55.66 mm and 29.66 mm (Figure 5). According to statistical analysis, MRSA

https://doi.org/10.1021/acsomega.4c00315
ACS Omega 2024, 9, 27030−27046

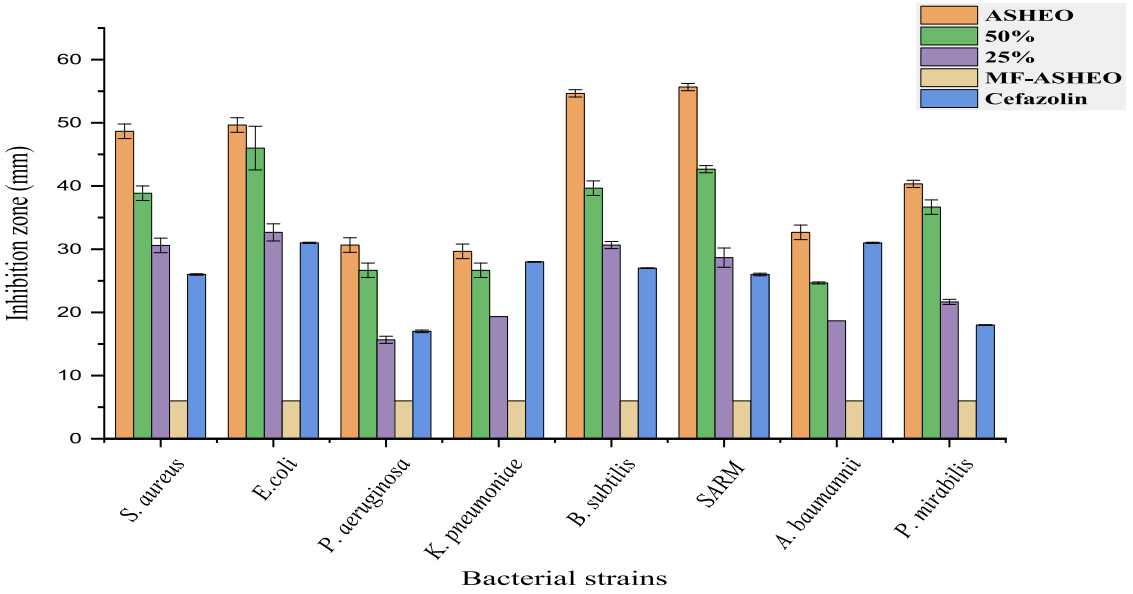

Figure 5. Antibacterial activity of ASHEO and MF-ASHEO using the disc diffusion method.

and *Bacillus subtilis* were the most sensitive, followed by *Escherichia coli*, *Staphylococcus aureus*, *Proteus mirabilis*, and *Acinetobacter baumannii*, while *Pseudomonas aeruginosa* and *Klebsiella pneumoniae* were less sensitive. In contrast, MF-ASHEO did not show any inhibition activity.

2.4.2. MICs. The minimum inhibitory concentrations (MICs) of ASHEO were evaluated against both reference strains and clinical isolates; as reported in Table 4, MIC values ranged from 0.031 to 0.125 mg/mL. ASHEO exhibited the lowest MIC against *S. aureus* and *B. subtilis* (0.031 mg/mL), whereas the highest MIC values were observed against *P. aeruginosa* and *A. baumannii* (0.125 mg/mL). Conversely, *E. coli*, *K. pneumoniae*, MRSA, and *P. mirabilis* demonstrated identical MICs (0.062 mg/mL).

Table 4. MICs of ASHEO against the Bacterial Strains

bacterial strains	MIC (mg/mL)	bacterial strains	MIC (mg/mL)
S. aureus	0.031	*B. subtilis*	0.031
E. coli	0.062	MRSA	0.062
P. aeruginosa	0.125	*A. baumannii*	0.125
K. pneumoniae	0.062	*P. mirabilis*	0.062

2.5. Antibiofilm Activity. In the CV assay, ASHEO substantially inhibited the development of biofilms of all of the bacteria, which agreed with the results mentioned above of the antibacterial activity. Notably, the absence of any inhibition effect for MF-ASHEO against the tested bacterial strains, as presented above, explains its exclusion from the test, as shown in Figure 6. ASHEO was able to effectively suppress the biofilm formation of *K. pneumoniae* at MIC/2 (0.0625 mg/mL), MIC/4 (0.0312 mg/mL), and MIC/8 (0.0156 mg/mL) concentrations compared to the control (samples without the EO) as presented in Figure 7. In the case of *A. baumannii*, our findings

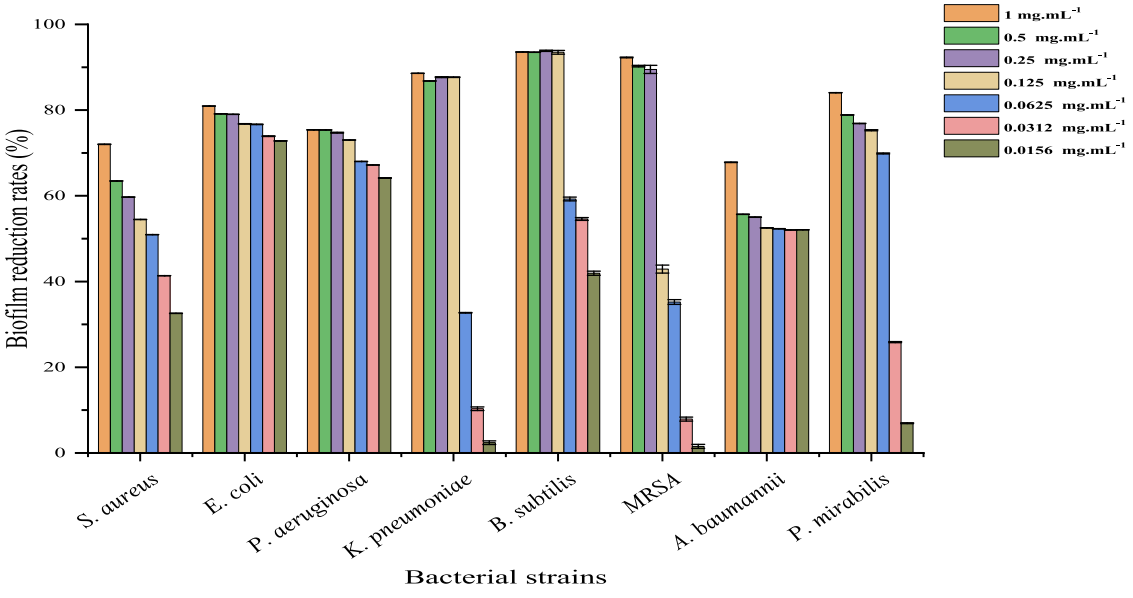

Figure 6. Biofilm reduction rates produced by ASHEO.

https://doi.org/10.1021/acsomega.4c00315
ACS Omega 2024, 9, 27030−27046

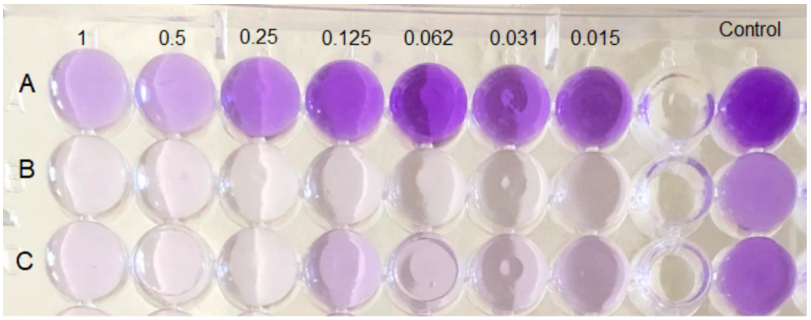

Figure 7. ASHEO's antibiofilm activity against (A) *P. aeruginosa*, (B) *A. baumannii*, and (C) *P. mirabilis*. Biofilm formation is visually indicated by the varying intensities of violet color on the test plate, progressing from left to right (wells 1−7), with concentrations in mg/mL. The ninth well serves as the control.

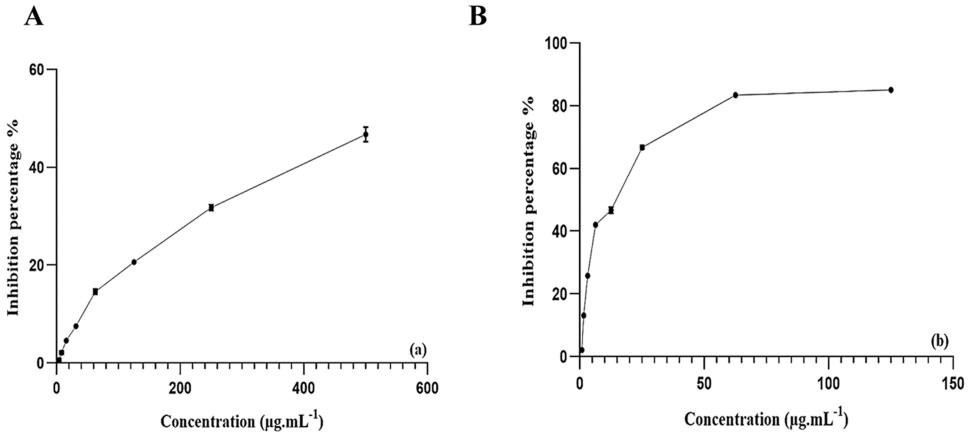

Figure 8. Free radical scavenging activity of ASHEO (A) and BHT (B).

demonstrated that each of the tested concentrations (MIC, MIC/2, MIC/4, and MIC/8) of ASHEO effectively prevented biofilm development. A significant reduction in biofilm formation was observed with *K. pneumoniae*, *A. baumannii*, and *E. coli*, achieving reductions of 72.8, 64.15, and 52.08%, respectively, at a concentration of 0.015 mg/mL (sub-MICs). The lowest reduction was detected for MRSA, *P. aeruginosa*, and *P. mirabilis* at the lowest concentration of ASHEO; however, the reduction exceeded 50% at an essential oil concentration of 0.125 mg/mL.

2.6. Free Radical Scavenging Activity. The antiradical activity is presented as the inhibition percentage at different concentrations of the samples (Figure 8). The inhibition percentage increased with the increase in concentration for both ASHEO and BHT. In contrast, MF-ASHEO showed no reductant activity in the DPPH assay. The ASHEO inhibited 46.70 ± 1.51% at 500 µg/mL concentration. However, BHT showed 85.00 ± 0.02% at only 125 µg/mL. The half-maximum inhibitory concentration (IC_{50}) of both samples is presented in Figure 9. The *t* test revealed significant differences between ASHEO and BHT ($p \leq 0.0001$). The IC_{50} was 536.47 ± 21.99 and 15.48 ± 0.06 µg/mL for ASHEO and BHT, respectively.

2.7. Antifungal Activities of ASHEO and MF-ASHEO. The antifungal impact of ASHEO and MF-ASHEO was evaluated against 10 strains of toxigenic fungi (Table 5). It was noticed that the antifungal effect was enhanced by applying the microfluidized technique. Compared to the standard antifungal (fluconazole), the inhibition zone of fungi was recorded to be closer to half of the standard effect. Moreover, the antifungal impact on the toxigenic fungal strains is ordered ascending as

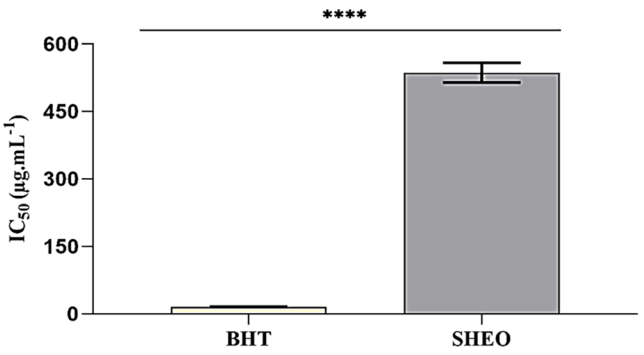

Figure 9. IC_{50} of ASHEO and BHT.

Aspergillus < *Fusarium* < *Penicillium*. It was noticed from the results in Table 5 that the inhibition zone diameter against the *Penicillium* fungi was recorded to be more than 50% (14.01 ± 0.34 to 16.11 ± 0.55 mm) compared to the fluconazole (26.51 ± 0.16 to 26.66 ± 0.21 mm). The zone of inhibition for some *Aspergillus* strains (*Aspergillus niger* and *Aspergillus carbonarius*) was recorded to be more than that for the other strains (*Aspergillus flavus*, *Aspergillus parasiticus*, and *Aspergillus ochraceous*).

The minimal fungicidal concentrations (MFCs) of ASHEO and MF-ASHEO were calculated as milligrams per liter (Table 5) against the standard fluconazole antifungal. The MFCs of the fluconazole against the 10 toxigenic strains ranged between 0.065 ± 0.001 and 0.079 ± 0.003 mg/L; these values ranged between 0.71 ± 0.04 and 1.02 ± 0.02 mg/L for the MF-ASHEO. A higher concentration was required for the ASHEO

https://doi.org/10.1021/acsomega.4c00315
ACS Omega 2024, 9, 27030−27046

Table 5. Antifungal Activities and Minimal Antifungal Concentrations of ASHEO and MF-ASHEO[a]

	part A			part B		
	inhibition zone (mm)			MFC (mg/L)		
fungal strains	ASHEO	MF-oil	ST	ASHEO	MF-oil	ST
A. flavus ITEM 698	8.37 ± 1.02^{b}	9.16 ± 0.94^{b}	23.21 ± 0.26^{a}	1.63 ± 0.18^{z}	1.02 ± 0.02^{y}	0.074 ± 0.004^{x}
A. parasiticus ITEM 11	6.05 ± 0.36^{b}	6.55 ± 0.41^{b}	26.08 ± 0.21^{a}	1.61 ± 0.26^{z}	1.01 ± 0.05^{y}	0.068 ± 0.002^{x}
A. ochraceous ITEM 5117	8.37 ± 0.53^{c}	9.47 ± 0.26^{b}	23.37 ± 0.31^{a}	1.39 ± 0.25^{z}	0.97 ± 0.05^{y}	0.076 ± 0.001^{x}
A. niger ITEM B5	10.21 ± 0.34^{b}	10.71 ± 0.28^{b}	26.15 ± 0.34^{a}	1.43 ± 0.17^{z}	0.74 ± 0.11^{y}	0.079 ± 0.003^{x}
A. carbonarius ITEM 5010	9.45 ± 0.55^{c}	10.85 ± 0.31^{b}	25.95 ± 0.24^{a}	1.39 ± 0.22^{z}	0.87 ± 0.14^{y}	0.078 ± 0.003^{x}
Penicillium verrucosum NRRL 695	14.26 ± 0.42^{b}	14.51 ± 0.77^{b}	26.66 ± 0.21^{a}	1.26 ± 0.14^{z}	0.61 ± 0.09^{y}	0.072 ± 0.001^{x}
Penicillium chrysogenum ATCC 48271	14.01 ± 0.34^{c}	16.11 ± 0.55^{b}	26.51 ± 0.16^{a}	1.29 ± 0.09^{z}	0.66 ± 0.12^{y}	0.071 ± 0.001^{x}
Fusarium graminearum ATCC 56091	11.05 ± 0.64^{c}	12.45 ± 0.34^{b}	25.22 ± 0.21^{a}	1.21 ± 0.15^{z}	0.71 ± 0.05^{y}	0.065 ± 0.001^{x}
Fusarium moniliforme ITEM 52539	10.63 ± 0.47^{c}	12.33 ± 0.21^{b}	26.63 ± 0.28^{a}	1.23 ± 0.11^{z}	0.74 ± 0.02^{y}	0.065 ± 0.001^{x}
Fusarium oxysporum ITEM 12591	10.18 ± 0.66^{c}	11.98 ± 0.37^{b}	26.54 ± 0.24^{a}	1.29 ± 0.05^{z}	0.71 ± 0.04^{y}	0.066 ± 0.001^{x}

[a]The results are expressed in mean ± SD (n = 5; $P \leq 0.05$). Data with different superscript letters significantly differ in the same row for each table part. *A*: *Aspergillus* fungi; *P*: *Penicillium* fungi; *F*: *Fusarium* fungi; ST: standard antifungal fluconazole.

Table 6. Antifungal and Antimycotoxigenic Impact of ASHEO and MF-ASHEO[a]

mycelial inhibition	mycelial growth (g)		inhibition (%)		
		A. parasiticus			
control	6.0856 ± 0.5771		--		
ASHEO	4.0041 ± 0.374		34.2%		
MF-ASHEO	3.1181 ± 0.4552		48.76%		
		P. verrucosum			
control	5.8247 ± 0.6221		--		
ASHEO	2.9828 ± 0.3711		48.79%		
MF-ASHEO	1.0774 ± 0.333		81.50%		
		Antimycotoxigenic (μg/L)			
mycotoxins	AFB_1	AFB_2	AFG_1	AFG_2	OCA
control	228.61 ± 5.16	218.11 ± 4.77	205.66 ± 5.37	201.41 ± 6.05	578.26 ± 7.27
ASHEO	127.11 ± 4.21	120.21 ± 5.31	113.66 ± 4.37	109.29 ± 5.21	269.24 ± 7.26
MF-ASHEO	24.28 ± 2.05	ND	19.55 ± 2.18	ND	ND
		Antimycotoxigenic ratio (%)			
mycotoxins	AFB_1	AFB_2	AFG_1	AFG_2	OCA
control	0	0	0	0	0
ASHEO	44.39 ± 0.57%	44.89 ± 1.21%	44.73 ± 0.66%	45.74 ± 0.94%	53.44 ± 0.67%
MF-ASHEO	89.38 ± 0.66%	100%	90.49 ± 0.79%	100%	100%

[a]The results are expressed as mean ± SD (n = 5; $P < 0.05$). ND: not detected. The reduction of mycotoxin production in medium is measured in (μg/L), and the reduction ratio is calculated as a percentage. AFB1: aflatoxin B1; AFB2: aflatoxin B2; AFG1: aflatoxin G1; AFG2: aflatoxin G2; and OCA: ochratoxin A.

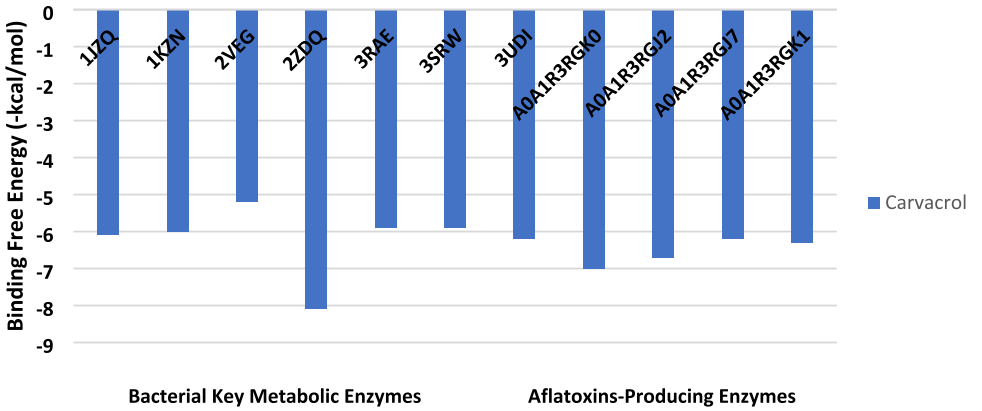

Figure 10. Binding free energy values were computed by molecular docking of carvacrol to bacterial metabolic and aflatoxin-producing enzyme receptors.

to achieve the inhibition, ranging between 1.21 ± 0.15 and 1.62 ± 0.25 mg/L. It was noticed that the microfluidizing technique influences the MFC concentration required to inhibit the growth of toxigenic fungi. This influence

https://doi.org/10.1021/acsomega.4c00315
ACS Omega 2024, 9, 27030−27046

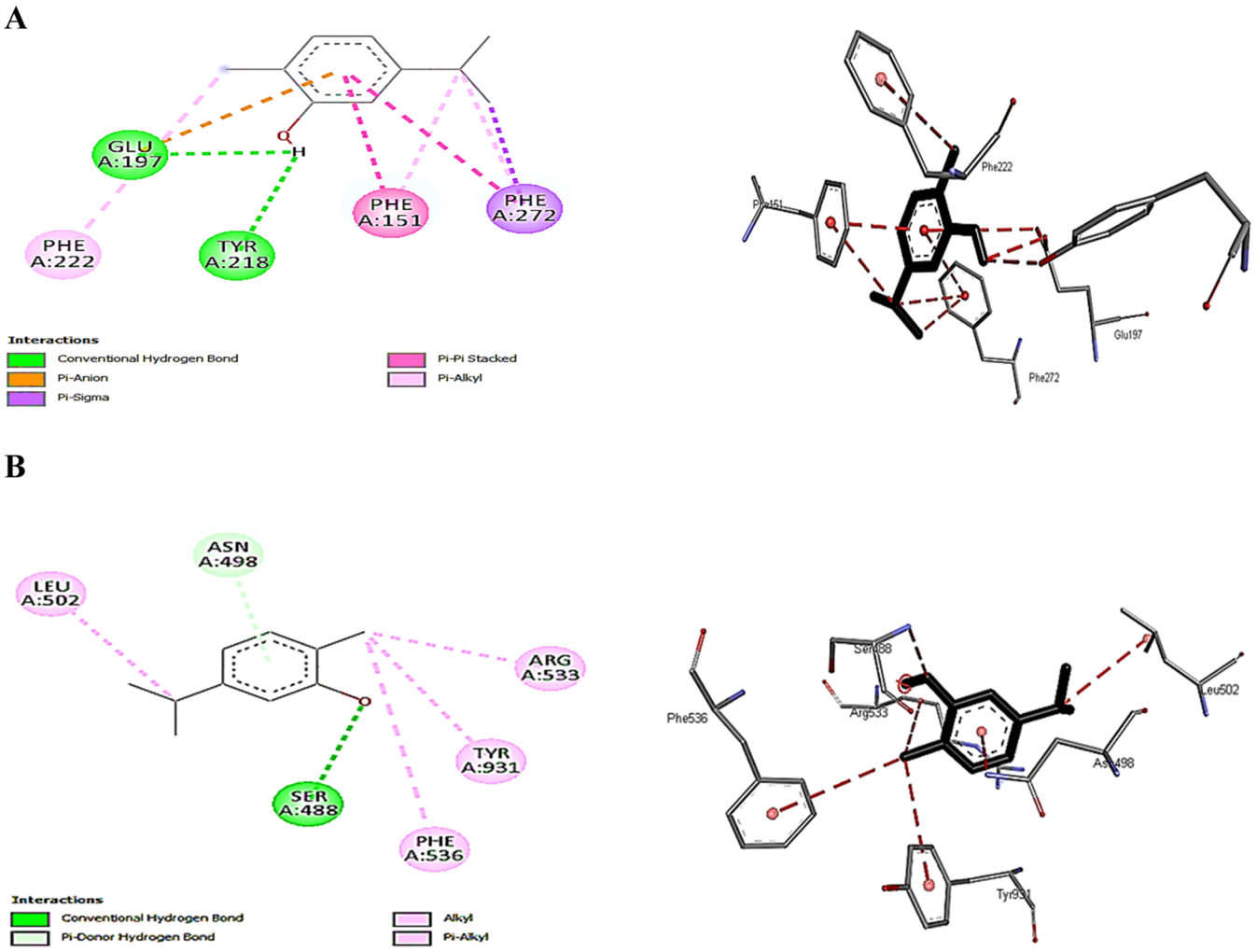

Figure 11. Interactions of carvacrol with 2ZDQ (A) and A0A1R3RGK0 (B).

ameliorates the inhibition by reducing the required concentration of the Algerian *S. hortensis* essential oil as MF-ASHEO.

2.8. Antifungal Impact in Simulated Media. The antifungal effect of ASHEO and MF-ASHEO was determined in simulated media (Table 6) against two strains, *A. parasiticus* and *P. verrucosum*. These strains were chosen for their ability to produce mycotoxins. The produced aflatoxins (AFB_1, AFB_2, AFG_1, and AFG_2) from the *A. parasiticus* strain were recorded by reduction if the medium growth contained ASHEO. This reduction was increased by applying a microfluidized form in media. The reduction ratio ranged between 44.39 ± 0.57 and 45.74 ± 0.94% regarding the four types of aflatoxins. The reduction ratio increased to 89.38 ± 0.66 and 90.49 ± 0.79% for AFB_1 and AFG_1, respectively.

The reduction was recorded entirely for the amount of AFB_2 and AFG_2. At the same time, the reduction recorded in mycelial growth of the fungus was 34.2 and 48.76% for medium containing ASHEO and MF-ASHEO, respectively. The inhibition recorded for the mycelia of *P. verrucosum* was between 48.79% for crude oil of Algerian *S. hortensis* and 81.50% for microfluidized ASHEO applied in medium growth of fungi. Otherwise, the reduction in ochratoxin A determined in the growth medium was up to complete reduction in the MF-ASHEO medium.

2.9. Molecular Docking and ADME Study. Carvacrol, the primary volatile component of the oil being studied, was investigated for its antibacterial and antiaflatoxigenic properties using a molecular docking approach. The results obtained from this study showed that carvacrol binds to critical enzymes that play a key role in the biosynthesis and repair of cell walls, proteins, and nucleic acids. The enzymes were identified by their PDB IDs: 1JZQ, 1KZN, 2VEG, 2ZDQ, 3RAE, 3SRW, and 3UDI. The binding free energies (ΔG) are displayed in Figure 10. The molecular docking analysis provided the best possible poses or positions of the ligand at the receptor site. A lower ΔG indicates a more vital interaction between the receptor and the ligand. Carvacrol showed binding affinities that ranged from −5.2 to −8.1 kcal/mol. The highest docking scores were observed for 2ZDQ (Figure 10). Similar results were obtained for the affinities toward enzymes responsible for producing aflatoxins. The enzymes studied were polyketide synthase (A0A1R3RGK0), nonribosomal peptide synthase (A0A1R3RGK1), cytochrome P450 monooxygenase (A0A1R3RGJ7), and halogenase (A0A1R3RGJ2). Among these enzymes, the highest affinity was observed between carvacrol and polyketide synthase with a binding energy of −7.0 kcal/mol, as shown in Figure 10.

In Figure 11A,B, we can see how carvacrol interacts with the crystal structure of polyketide synthase (A0A1R3RGK0) and D-alanine: D-alanine ligase (PDB: 2ZDQ). These interactions show the highest docking scores. The reason behind the higher binding affinity of carvacrol with 2ZDQ (−8.1 kcal/mol) is

https://doi.org/10.1021/acsomega.4c00315
ACS Omega 2024, 9, 27030−27046

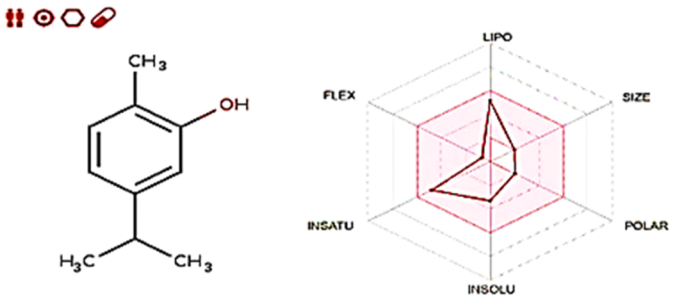

SMILES CC(c1ccc(c(c1)O)C)C

Physicochemical Properties	
Formula	C10H14O
Molecular weight	150.22 g/mol
Num. heavy atoms	11
Num. arom. heavy atoms	6
Fraction Csp3	0.40
Num. rotatable bonds	1
Num. H-bond acceptors	1
Num. H-bond donors	1
Molar Refractivity	48.01
TPSA	20.23 Å²
Lipophilicity	
Log $P_{o/w}$ (iLOGP)	2.24
Log $P_{o/w}$ (XLOGP3)	3.49
Log $P_{o/w}$ (WLOGP)	2.82
Log $P_{o/w}$ (MLOGP)	2.76
Log $P_{o/w}$ (SILICOS-IT)	2.79
Consensus Log $P_{o/w}$	2.82

Water Solubility	
Log *S* (ESOL)	-3.31
Solubility	7.40e-02 mg/ml ; 4.92e-04 mol/l
Class	Soluble
Log *S* (Ali)	-3.60
Solubility	3.79e-02 mg/ml ; 2.53e-04 mol/l
Class	Soluble
Log *S* (SILICOS-IT)	-3.01
Solubility	1.46e-01 mg/ml ; 9.71e-04 mol/l
Class	Soluble
Pharmacokinetics	
GI absorption	High
BBB permeant	Yes
P-gp substrate	No
CYP1A2 inhibitor	Yes
CYP2C19 inhibitor	No
CYP2C9 inhibitor	No
CYP2D6 inhibitor	No
CYP3A4 inhibitor	No
Log K_p (skin permeation)	-4.74 cm/s
Druglikeness	
Lipinski	Yes; 0 violation
Ghose	No; 1 violation: MW<160
Veber	Yes
Egan	Yes
Muegge	No; 2 violations: MW<200, Heteroatoms<2
Bioavailability Score	0.55
Medicinal Chemistry	
PAINS	0 alert
Brenk	0 alert
Leadlikeness	No; 1 violation: MW<250
Synthetic accessibility	1.00

Figure 12. *In silico* ADME properties of carvacrol using SwissADME.

attributed to the conventional hydrogen bonding from carvacrol (H-donor) to the O-of GLU A:197 and OH-group of TYR A:218 (H-acceptors) as shown in Figure 11A. The distances in hydrogen bonds observed in the study ranged from 2.4 to 2.7 Å. Apart from these hydrogen bonds, other interactions are observed between 2zdq residues and carvacrol. These interactions include π−anion, $\pi-\sigma$, and $\pi-\pi$ stacked and π-alkyl electrostatic and hydrophobic interactions (Figure 11A). The only electrostatic bond of the π−anion type is formed between the negative O-of GLU A:197 and π-orbitals of carvacrol. The $\pi-\sigma$ hydrophobic interaction is from the C−H of carvacrol to π-orbitals of PHE A:272. The study also revealed that carvacrol alkyl groups interact with aryl-containing amino acids such as PHE A:151, 222, and 272 through their π-orbitals (Figure 11A). Additionally, a $\pi-\pi$ stacked interaction is the attractive force between aromatic rings due to the presence of π-electron clouds like the π-orbitals of PHE A:151 and 272 and carvacrol.

Only one conventional solid hydrogen bond was observed between carvacrol and polyketide synthase (A0A1R3RGK0), which is responsible for the lower free binding energy (−7.0 kcal/mol). A weak hydrogen bond in the shape of the π-donor interaction from the ASN A:498 (H-donor) to the π-orbitals of carvacrol could be observed. (Figure 11B). In addition, alkyl hydrophobic interactions were detected from carvacrol to the enzyme residues ARG A:533 and LEY A:502. Finally, π-alkyl hydrophobic interactions were conducted from the π-orbitals of PHE A:536 and TYR A:931 to the carvacrol alkyl group (Figure 11B).

SwissADME analyzed the ADME properties of carvacrol and found that it has a molecular weight of less than 500. It also has less than five hydrogen bond donors, acceptors, and log *p* values. The value of log *p* is responsible for transportation, indicating hydrophobicity and lipophilicity. The topological polar surface area (TPSA) and rotatable bond also fall within acceptable limits. Carvacrol has adequate hydrophobic and moderate lipophilic properties, allowing it to cross the membrane surface and reach the receptor site quickly. Additionally, its log *S* value is within an acceptable range, meaning that it is highly absorbable in the gastrointestinal tract. Solubility (log *S*) significantly affects its absorption and distribution features. Furthermore, carvacrol exhibits drug-like properties and follows Lipinski's rule of 5, as shown in Figure 12.

3. DISCUSSION

Studying the chemical composition of essential oil extracted from the Algerian cultivar of *S. hortensis* L. (Table 1) allows us to know its potential use in various applications such as foods, pharmaceuticals, biopreservation, cosmetics, etc.[12] The extraction process of the present study resulted in a yield of 2.78%, which is higher than that obtained in other Algerian regions like Tizi-Ouzou (0.06%), Bordj-Ménaïel (2.2%), and jedioua Relizane (0.68%), as reported by Djenane et al.[6,13] and Chouitah et al.[7] At the same time, no data are available in the literature about the extraction yield of ASHEO collected from Bou Saada, M'Sila Province in Algeria. Many factors affect the oil yield and the plant's productivity, such as age, genotype, agronomics, climate, and the harvesting period, Djenane et al.[6]

https://doi.org/10.1021/acsomega.4c00315
ACS Omega 2024, 9, 27030−27046

Compared to the literature dealing with AHEO reported before, the present study's findings agree with Djenane et al.[6] regarding the volatile profile of ASHEO, with carvacrol, γ-terpinene, and p-cymene as the predominant compounds. In contrast, Chouitah et al.[7] showed a different ASHEO chemotype, where cadinol, thymol, himachalene, and selinene were the major constituents of the volatile fraction. The ASHEO of the present study showed a higher concentration of monoterpenes, accounting for 92.67%, which is close to the findings of Chambre et al.[4] in Romania, where the total monoterpenes were 96.99%. Typically, and in agreement with our findings, essential oils of *S. hortensis* L. from various locations in Turkey and other regions have shown higher levels of carvacrol than those of thymol.[14,15] Nevertheless, specific chemotypes of this species have been documented in Turkey[16] and Libya,[17] where thymol constitutes the major component. Area, climate, and seasonal factors can influence the composition of the essential oil content. An example of this influence is demonstrated in the research by Baher et al.,[18] where severe water stress was observed to cause alterations in the contents of carvacrol and γ-terpinene.

Energy-intensive approaches like high-pressure homogenization can alter the composition of essential oils, increasing some components but decreasing others. For instance, in the Algerian *Saccocalyx satureioides* oil nanoemulsion, thymol and carvacrol were more abundant at the expense of borneol and α-terpineol concentrations found in the hydrodistilled oil.[19] In the same line, using microfluidization as a high-pressure homogenization technique in the present study leads to a dramatic increase in the carvacrol content (94.51%) at the expense of both γ-terpinene and *p*-cymene, as shown in Table 1. Chambre et al.[4] conducted an extensive heating treatment on *S. hortensis* L. oil to determine its effect on the γ-terpinene and carvacrol concentrations under different temperatures (160, 175, 190 °C) and durations (0.5 and 2.5 h). The heating treatment caused a decrease in the γ-terpinene content, while the carvacrol concentration increased depending on the temperature and heating time. It was discovered that γ-terpinene is a precursor of carvacrol and is converted to p-cymene and then carvacrol through aromatization and hydroxylation processes during storage at different temperatures and times.[11] Our findings are consistent with this hypothesis, in which carvacrol had an inverse relationship with its precursor, γ-terpinene, during microfluidization. The bioactivity of carvacrol as an antioxidant, antimicrobial, antiparasitic, anti-inflammatory, antinociceptive, hepatoprotective, anticancer, and pain management agent makes it a valuable ingredient in various sectors such as food and pharmaceuticals.[4] However, further studies are needed to understand the mechanisms of transferring volatile compounds during energy-intensive processes.

The operating pressure affects the mean droplet diameter and the PDI of nanoemulsions. In agreement with the present study's findings (Figure 2), higher pressure results in smaller droplets, with the smallest observed at 150 MPa.[20] However, droplet size can increase during production due to collision and coalescence caused by strong Brownian movement and weak surfactant adsorption at higher pressure. For example, nanoemulsions with D-limonene and terpenes were treated at 300 MPa for 10 cycles, resulting in droplet sizes ranging from 74.4 to 356.7 nm.[21] In addition to the operating pressure, the carvacrol−surfactant interaction and adsorption of Tween80 into the MF-ASHEO nanoemulsion were responsible for the lower droplet size.[22] It is believed that the phenol group of carvacrol, the major component in MF-ASHEO at 94.51%, is located on the surface of the oil droplet, oriented toward the water. This provides flexibility for the interphase, allowing for stronger compaction of the surfactant mixture. Different-sized molecules of amphiphilic compounds can achieve better packaging and stabilize the interfaces more effectively.

As a result, better adsorption led to a higher decrease in interfacial tension, resulting in smaller droplets for MF-ASHEO.[23] Thymol, a carvacrol isomer, can be solubilized in various locations within Tween 80 micelles, such as the micelle−water interface, between hydrophilic head groups, in the palisade layer, and the inner hydrophobic core. Thymol molecules are found at the junction of hydrophilic head groups and the palisade layer, enabling them to interact directly with Tween 80 monomers. After solubilization, 1H NMR spectra indicated significant upfield shifts in three of thymol's seven types of protons. These shifted protons were all on the benzene ring, with 3-H and 4-H exhibiting more significant shifts, indicating an interaction with the ester group of Tween 80.[24] Therefore, despite the optimization based on operational conditions noted in the literature, the surfactant (Tween 80)-to-oil ratio was fixed at 1:1, which was applied in the current study.[8,22]

The microfluidization process caused a significant reduction in the ζ-potential of MF-ASHEO droplets to −39.4 mV, which indicates an increase in their net electrical charge (Figure 2B). When the ζ-potential of droplets falls below ±30 mV, the repulsive forces between droplets in the nanoemulsion are weakened and may cause instability.[25] The nonionic emulsifier/surfactant Tween 80 gives oil droplets a negative charge by selectively adsorbing hydroxyl ions from the aqueous phase or anionic impurities like free fatty acids in the oil or surfactant phases.[26] The anionic hydrocolloid CMC confers a negative ζ-potential to nanoemulsions, which helps stabilize them. The stability of the nanoemulsion depends on the interactions and competition with species that have already been adsorbed.[27] The difference in the ζ-potential of emulsions and nanoemulsions containing different essential oils could be due to variations in ionizable oil compounds.[28] The MF-ASHEO nanoemulsion has a lower negative ζ-potential than that of Algerian lemongrass oil, with citral isomers as the major constituents.[8]

Materials and biological samples have been imaged using TEM to investigate the shape and structure of the nanoemulsion (Figure 3). According to the literature, the particle sizes determined by the TEM are supposed to be smaller than those specified by the DLS instrument due to air-drying the emulsion during preparation. Nevertheless, the current study shows that oil droplet aggregation or destruction must be expected under electron microscopy's dehydration conditions.[29] In agreement with Boudechicha et al.,[8] who used the same technique to encapsulate Algerian lemongrass oil, the morphological characterization of the MF-ASHEO nanoemulsion showed that nanoparticles appeared to be round in shape, in a good dispersion, and in narrow size distribution, which proved the efficiency of the microfluidization process as a successful nanoencapsulation technique for ASHEO.

To the best of our knowledge, a few studies dealing with the cytotoxicity of *S. hortensis* L. volatile oil have been published, but nothing has been published concerning Algerian oils or nanoemulsion activity. The cytotoxic impacts recorded for the present ASHEO agreed with Popovici et al.,[30] where the oil

https://doi.org/10.1021/acsomega.4c00315
ACS Omega 2024, 9, 27030−27046

showed concentration-dependent activity and greater efficacy than the hydroethanolic extract on both tumor cell lines, A375 (IC_{50} 22.27 μM) and B164A5 (IC_{50}, 34.16 μM), using MTT assay.

It is worth highlighting that MF-ASHEO showed lesser cytotoxicity than ASHEO after 24 h of exposure in this study. The entrapment of bioactive compounds in nanostructures can change their route of association or internalization to the targeted cell, which can explain the difference in cytotoxicity between ASHEO and MF-ASHEO *in vitro*.[31] This result is consistent with Milhomem-Paixão et al.[32] and da Silva Gündel et al.,[33] who studied the cytotoxicity of andiroba and basil oil nanoemulsions. According to Chime et al.,[34] an effective drug delivery system should maximize therapeutic benefits while minimizing toxicity. Our study found that using MF-ASHEO as a delivery system improved drug efficacy, reducing the necessary concentration while maintaining effectiveness and minimizing side effects. Notably, low cytotoxicity in normal cells does not necessarily mean reduced bioavailability of bioactive compounds *in vivo*. Nanostructures can accumulate in the desired target by taking advantage of the unique characteristics of the pathological process when used for therapeutic purposes. For example, nanoparticles can accumulate preferentially in inflammatory lesions due to abnormal blood vessels and reduced lymphatic drainage. This passive accumulation is known as the EPR effect (enhanced permeation and retention), which helps increase the amount of bioactive compounds in the desired target.[35]

It is known that the hydrophobic properties of essential oil components allow them to distribute into the lipids of bacterial cell membranes, causing disruptions in their arrangement and enhancing their permeability.[36] In this study, all tested strains exhibited sensitivity to ASHEO (Table 3). These findings are mainly attributed to the high content of carvacrol, which is one of the key active constituents of essential oils.[37] This also aligns with the outcomes reported for *S. hortensis* and *Satureja montana* essential oils with high carvacrol concentration. These oils demonstrated higher antimicrobial effectiveness than that of essential oils containing lower amounts of carvacrol.[38] The abundant presence of phenolic compounds, such as carvacrol and thymol, within the essential oil of *Satureja* spp. is extensively documented as a defining factor for strong antimicrobial effectiveness.[39] The current study confirmed the antibacterial efficacy of ASHEO against the reference and clinical isolates. These results agree with a different investigation involving *S. hortensis* and *S. montana* essential oils, which reported similar MICs.[13] ASHEO displayed intense activity with low MIC values; it was about 0.125 mg/mL against *P. aeruginosa* and 0.031 mg/mL against *S. aureus* and *B. subtilis* (Table 4).

In contrast, it was relatively weak in the study conducted by Abou Baker et al.,[36] where the essential oil from *S. hortensis* exhibited MIC values of 3 mg/mL against *P. aeruginosa* and 2 mg/mL against *S. aureus*. In agreement with Sharma et al.,[40] who reported the absence of inhibitory properties for the nanoemulsions made with Tween 80 and *Eucalyptus globulus* essential oil, no antibacterial activity could be observed for MF-ASHEO. This could be due to the low oil concentration in the nanoemulsion formula (1%), the physicochemical properties that may influence the nanoemulsions' antimicrobial properties, and the limited incubation time.[41] Therefore, further improvements should be applied to improve the antimicrobial properties of the nanoemulsion formed.

Bacterial biofilm formation is now considered to be one of the most important virulence factors. They are associated with millions of hospital-acquired infections annually, incurring an annual economic burden of billions of dollars. The development of bacterial biofilms can confer unique traits to the bacterial cells, such as enhanced resistance to antimicrobial agents; the search for novel agents effective against biofilms is of immense importance.[42] Based on the obtained results in this study, we conclude that ASHEO exhibited significant antibiofilm activity against all tested biofilm-producing strains (Figures 6 and 7). Diverse investigations have revealed *Satureja* spp.'s potential to counteract biofilm formation by both bacterial and fungal strains.[43] Specifically, in a notable instance, Sharifi et al.[44] observed a significant effect of sub-MIC *S. hortensis* essential oil on preventing biofilm formation by *S. aureus* and disrupting the pre-existing biofilms. They proposed that the primary contributors to the oil's antibiofilm and antiadhesive properties are likely the thymol and terpinene compounds in *S. hortensis* essential oil.

The ASHEO and BHT standards were shown to be effective DPPH scavengers. The obtained IC_{50} values were in the order BHT < ASHEO (Figure 8). The potent antioxidant activity of ASHEO could be attributed to its high terpene content,[45] mainly monoterpene hydrocarbons and oxygenated monoterpenes, as determined earlier. These compounds can donate protons to stabilize free radicals.[4] This study's results agree with those conducted on *S. hortensis* L. essential oil by Baker et al.[36] *S. montana* L. essential oil also showed a strong radical scavenging capacity.[46] The absence of reductant activity in the DPPH assay for MF-ASHEO may be due to the antioxidant compounds being encapsulated in the nanoemulsions, hindering their release and interaction with the chemical agent. Although the DPPH test indicates that the nanoemulsions did not exhibit reductive activity, they may still have antioxidant activity.[47] Ha et al.[48] found that the incubation period of a sample with the reagent can impact the release of encapsulated compounds in some nanoemulsions. In the current study, the active principles may not have been released in the nanoemulsions due to the relatively short incubation period. The expression values for the reductive activity evinced this.

Lately, there has been growing interest in investigating the potential of natural compounds as alternatives to conventional chemicals to mitigate the adverse effects of food loss and contamination, thereby decreasing our dependence on existing chemicals. The postharvest degradation in crop contamination by toxigenic fungi and mycotoxins leads to substantial reductions in yield. Physical or chemical approaches may effectively manage fungal development in crops during storage. Various techniques are used to mitigate mycotoxin contamination and the accompanying fungal proliferation on dietary substances. Our results show the positive impact of the essential oil obtained from the Algerian *S. hortensis* plant against 10 strains of mycotoxigenic fungi (Table 5). These results follow the previous findings reported for the plant from different places[10] and may even change the inhibition ratio. Other investigations were linked between essential oils in fungal growth media and the mutation that could occur for toxin-producing genes. The impact in some cases was illustrated as an impact of special volatiles, such as carvacrol and thymol. Also, the carvacrol impact of inhibition for *Fusarium* fungi was reported as significant in a previous investigation.[49]

https://doi.org/10.1021/acsomega.4c00315
ACS Omega 2024, 9, 27030−27046

Moreover, a combination of carvacrol or thymol and the standard materials of antibiotics or antifungals was reported by significant inhibition.[50] The synergistic effect between carvacrol and thymol increased the antimicrobial potency against several microorganisms. This activity was reported to be caused by the presence of organic acids.[51] The present investigation recorded the amelioration of antifungal and antimycotoxigenic impact of *S. hortensis* L. essential oil by the microfluidization technique. Moreover, the reduction in aflatoxins and ochratoxin A production in simulated media was recorded as a decrease in significant values (Table 6). These results agreed with the previous results that referred to the enhancement of carvacrol and thymol by transforming their solution into nanoforms.[52] The nanoemulsion formed from carvacrol and thymol was reported by efficacy amelioration, particularly for its antimicrobial characteristics. In this regard, our investigation provides strong evidence for the correlation between microfluidization as a technique of nanoemulsion preparation and the ameliorative properties of Algerian *S. hortensis* L. essential oil, particularly for biological activities.

Hydrogen bonds in biological complexes play a critical role in molecular recognition specificity. They have an associated free energy ranging from −1.5 to −4.7 kcal/mol.[53] Weak hydrogen bonds include C−H···π-interactions that contribute significantly to protein stability.[54] Carvacrol alkyl groups commonly interact with aryl-containing amino acids like PHE through its π-orbitals. Hydrophobic interactions between aliphatic and aromatic carbons are the most common in protein−ligand complexes, with benzene rings being the most common aromatic system (Figure 11).[53]

To the best of our knowledge, there are no previous reports on the *in silico* investigation of carvacrol and its effects on enzymes associated with bactericidal/bacteriostatic effects or aflatoxin biosynthesis, which is discussed in the current study. However, a similar *in silico* study of carvacrol, the major component of *Origanum compactum* Benth oil, showed comparable activity against nicotinamide adenine dinucleotide phosphate oxidase (2CDU) and *S. aureus* nucleoside diphosphate kinase (3Q8U) with a glide score of −6.082 and −6.039 kcal/mol, respectively.[55] The free energy (ΔG kcal/mol) obtained from experiments showed that carvacrol has a stable binding affinity (−5.5 to −5.6 kcal/mol) with extended-spectrum β-lactamase (ESBL) enzyme-producing *E. coli*, such as TEM-72, SHV-2, and CTXM-9. The hydrogen bonds with amino acids in ESBL proteins anchor the protein residues and contribute to their interactions with carvacrol. Additionally, hydrophobic interactions are crucial to ligand−protein interactions. Carvacrol exhibited five hydrophobic interactions with TEM-72, two with SHV-2, and three with CTXM-9.[56]

Early prediction of drug-like filters is important in optimizing small molecules for therapy and increasing their chances of becoming a successful drug. These filters are based on empirical rules focusing on key pharmacokinetic indices, providing crucial information for drug discovery. In this regard, Figure 12 shows the essential druglikeness filters for carvacrol, which is recommended as a potential candidate for cancer drug design by SwissADME. According to Lipinski's rule of 5, which allows for no more than one violation, the tested compound can be used as an orally dosed drug in humans. Additionally, carvacrol exhibits high human intestinal absorption, making it a viable option for oral administration. The ADME analysis of this study is consistent with previous research done by Herrera-Calderon et al.,[57] who studied the mechanism of action of carvacrol on different receptors involved in breast cancer progression and its potential as an anticancer agent. Given these pharmacokinetic properties, carvacrol could be a promising therapeutic alternative for antibacterial or antifungal treatments.

The present study's findings suggest that the microfluidization process can dramatically affect the volatile content with a reverse relation between oxygenated and nonoxygenated terpenes. In addition, the degree of entrapment and rate of release may affect the activity and the application in which the nanoemulsions may be used. In other words, intact time during experiments or applications related to the release rate makes the current study's antifungal activity a promising application. Therefore, further studies can be conducted to examine the effect of the microfluidization process on volatile compounds and discover the impact of different polymers that may be used as surfactants on the activity of the formulated nanoemulsion.

4. CONCLUSIONS

The use of microfluidization as a high-pressure homogenization to load the *S. hortensis* L. hydrodistilled oil in nanosystems has dramatically affected the volatile composition of the oil and its nanoemulsions, where oxygenated terpenes like carvacrol vastly increased at the expense of nonoxygenated ones, such as terpinene. The main particle size was 41.72 nm with a higher emulsion stability, where the PDI and ζ-potential were 0.291 and 39.4 mV, respectively. TEM micrographs revealed spherical nanoparticles with varying diameters in nm. Cytotoxicity of the oil and its microfluidized nanoemulsion against three cell line strains recorded promising values determined by two assays (MTT and WST-1) with higher selectivity using HepG2, Vero, and WI-38 cell lines. By evaluating the antibacterial activity, MRSA and *B. subtilis* were the most sensitive, followed by *E. coli*, *S. aureus*, *P. mirabilis*, and *A. baumannii*, against the oil, which agreed with the antibiofilm activity. Meanwhile, the microfluidic nanoemulsion did not show any inhibition activity. The same trend was shown when the free radicals were scavenged using the DPPH assay. In contrast, the microfluidized nanoemulsion enhanced the antifungal activity in the ascending order *Aspergillus* < *Fusarium* < *Penicillium*, which was also proved by reducing aflatoxins (AFB1, AFB2, AFG1, and AFG2) in simulated media. The molecular docking technique was used to study the interaction of carvacrol with the key enzymes involved in bactericidal/bacteriostatic effects and the aflatoxin biosynthesis pathway, where the highest binding free energy was shown against D-alanine: D-alanine ligase and polyketide synthase. Carvacrol exhibited drug-like properties and followed Lipinski's rule of 5 according to the calculated ADME investigation.

5. MATERIALS AND METHODS

5.1. Chemicals, Plant Material, and Essential Oil Extraction. All chemicals applied in this investigation were HPLC grade and purchased from Sigma-Aldrich, Saint Louis, MO. The used sample, scientifically referred to as *S. hortensis* L., the aerial part of this plant, consisting of stems, leaves, and flowers, was collected from Bou Saada, situated 245 km south of Algiers, Algeria. The specific geographical coordinates are a latitude of 35°17′02.4″ north and a longitude of 4°18′06.8″

https://doi.org/10.1021/acsomega.4c00315
ACS Omega 2024, 9, 27030−27046

east, with an elevation of 553 m above sea level. Prof. Hocine Laouer, Department of Biology and Plant Ecology, Setif-1 University, Algeria, conducted plant identification. A voucher specimen validating the plant's identity was placed in our laboratory herbarium and assigned the code SAS28/03/21. Then, the collected plant material was air-dried at ambient room temperature under shaded conditions.

The essential oil was extracted using the hydrodistillation method with the Clevenger apparatus. 100 g of sample and distilled water were boiled for 3 h. The oily phase was then condensed, and the essential oils were extracted, dried with anhydrous sodium sulfate, and stored in airtight glass vials sealed with aluminum foil at −20 °C until analysis. The experiment was repeated three times.[20]

5.2. ASHEO Nanoemulsion Preparation. The coarse emulsion was prepared by mixing carboxymethyl cellulose (CMC) solution (2%), essential oil (1% v/v), and Tween 80 (1% v/v) with a magnetic stirrer for 30 min. Then, it was fed into a microfluidization system (M110P, Microfluidics, Westwood, MA) at 150 MPa for five cycles to obtain the nanoemulsion form. At the outlet of the interaction chamber, the product was refrigerated through an external cooling coil immersed in a water bath with ice, keeping its temperature always below 15 °C. The final emulsion was refrigerated until further investigations.[8,58]

5.3. Characterizations of the ASHEO Nanoparticles. Physicochemical characterization, such as pH, density, refractive index, and stability test, was done only for microfluidic nanoemulsions since primary emulsions are prone to breakdown quickly. Stability was checked by centrifugation. The height was recorded after pouring 1 mL of samples into mini tubes. They were subjected to 15,115*g* for 1 min (Sigma 3−18 KS, Osterode am Harz, Germany). The height of the supernatant was recorded compared to the initial one.[22] The particle size distribution, polydispersity index (PDI), and ζ-potential of the microfluidic nanoemulsion sample were measured using a Zetasizer Nano ZS instrument (Nano-S90, Malvern Panalytical Ltd., U.K.) at a temperature of 25 ± 0.1 °C, with dilution using deionized water to avoid multiple scattering effects. The morphology of nanoemulsions was analyzed using transmission electron microscopy at 160 kV operation (JEOL Ltd., Tokyo, Japan). Samples were applied to a copper specimen grid (200 mesh), stained with 3% phosphotungstic acid, and observed under a transmission emission microscope or TEM.[8]

5.4. Gas Chromatography−Mass Spectrometry (GC−MS). The study aimed to investigate the impact of the microfluidization technique on ASHEO volatiles by performing a GC-MS analysis. The nanoemulsion was mixed with diethyl ether using a vortex mixer and transferred to a 2 mL screw-cap vial for analysis after settling and drying with anhydrous sodium sulfate anhydrous. All extraction steps were repeated three times.[8] The analysis of the volatile compounds in ASHEO and its nanoemulsion was carried out by using gas chromatography (Agilent 8890 GC System) coupled with a mass spectrometer (Agilent 5977B GC/MSD) equipped with an HP-5MS-fused silica capillary column (30 m, 0.25 mm inner diameter, 0.25 mm film thickness). The oven temperature was initially set at 50 °C and then programmed from 50 to 200 °C at a rate of 5 °C/min and from 200 to 280 °C at a rate of 10 °C/min and to isothermal for 7 min. The flow rate of helium was 1.0 mL/min. 1 μL of the sample was injected at 230 °C with a split ratio of 1:50. Mass spectra in electron impact mode (EI) were obtained at 70 eV and scanning m/z ranging from 39 to 500 amu. Peaks were identified by comparing them to NIST, standards, and published data. Percentages of the detected compounds were calculated by using GC peak areas. The Kovats index of each compound was determined using retention times of C_6−C_{26} *n*-alkanes and compared to literature values.[59]

5.5. Cytotoxicity of ASHEO and Its Microfluidized Nanoemulsion Using MTT and WST-1 Cell Viability Assays. HepG2, WI-38, and Vero cell lines were treated with oil and the nanoemulsion and then tested using an MTT assay. The cells were seeded at 1 × 105 cells/well density and cultured in DMEM with 10% PBS serum and antibiotics. The concentrations of the oil and nanoemulsion were serially diluted in the ranges of 0.097−1000 μg/mL for HepG2 and 31.25−1000 μg/mL for Vero and WI-38. Cisplatin was used as a positive control. The absorbance at 540 nm was measured by using a microplate reader (BMG LABTECH-FLUOstar Omega microplate reader, Ortenberg, Germany) after dissolving the formazan crystals in DMSO for 20 min. The proportion of surviving cells and IC_{50} were calculated using eq 1

$$[(OD_{sample} - OD_{blank})/(OD_{control} - OD_{blank}) \times 100\%] \quad (1)$$

where OD_{sample} is the optical density of the sample, OD blank is the optical density of the blank (DMSO), and OD control is the optical density of the control.

Cell viability was assessed using the WST-1 assay with an Abcam kit (ab155902 WST-1 Cell Proliferation Reagent). After seeding 3 × 103 cells in 96-well plates and incubating in complete media for 24 h, the cells were treated with oil or the nanoemulsion at various concentrations for 48 h and then exposed to 10 μL of WST-1 reagent. Cell viability was measured using a microplate reader.[60]

Morphological changes in cell lines treated with various concentrations of ASHEO and its nanoemulsions were evaluated using a Zeiss Axio Vert A1 microscope (Carl Zeiss Microscopy Gmbh, 07745 Jena, Germany) compared to the control.

5.6. Evaluation of Antibacterial Activity. The effects of ASHEO and MF-ASHEO on bacteria were evaluated using the agar diffusion method and broth microdilution assay. Eight species of bacteria were tested, including those causing human diseases and food poisoning: *E. coli* (ATCC 25922), *P. aeruginosa* (ATCC 27853), *K. pneumoniae* (ATCC 13883), *P. mirabilis* (clinical isolate), *A. baumannii* (clinical isolate), *B. subtilis* (ATCC 6633), *S. aureus* (ATCC 25923), and methicillin-resistant *S. aureus* (MRSA) (clinical isolate). Inhibition zone diameters were measured after 24 h of incubation at 37 °C. Results were compared to a positive control of cefazolin KZ (30 μg, UG LF9015, Liofilchem, Italy) and a negative control of DMSO. All assays were performed in triplicate.[61]

5.7. Minimum Inhibitory Concentration (MIC). MIC values of ASHEO were determined in triplicate using the broth microdilution method.[62] Each bacterial strain's suspension was adjusted to 0.5 McFarland and mixed with Muller Hinton Broth, EO (0.007−1 mg/mL), DMSO (0.1%), and TTC (0.05%). DMSO enhanced oil solubility, and TTC determined bacterial growth. The negative control was a well without a bacterial suspension. After an 18−24 h incubation at 37 °C, bacterial growth was evaluated.

https://doi.org/10.1021/acsomega.4c00315
ACS Omega 2024, 9, 27030−27046

5.8. Antibiofilm Activity. ASHEO's impact on bacterial biofilm formation was tested using the crystal violet assay previously described by Stepanovic et al.[63] In sterile 96-well polystyrene plates, 100 μL of MH broth with different concentrations of essential oil was added to 100 μL of the bacterial inoculum (adjusted to 10^9 CFU/mL). After 48 h of incubation at 37 °C, the wells were rinsed and stained with crystal violet (0.4%). Acetic acid (30%) was added to dissolve the stain. The absorbance was measured at 595 nm, and the percentage of inhibition was calculated using eq 2

$$\text{biofilm inhibition \%} = \frac{(\text{Abs negative control} - \text{Abs test})}{\text{Abs negative control}} \times 100 \quad (2)$$

5.9. Free Radical Scavenging Activity. ASHEO and MF-ASHEO's ability to scavenge free radicals was tested using DPPH, following Hatano et al.'s method.[64] ASHEO or BHT was added to a DPPH solution and incubated in the dark for 30 min. Absorbance was then measured at 517 nm by using a UV−Vis spectrophotometer (JASCO V-730 spectrophotometer, MD 21601). All tests were run in three replicates, and the results were averaged. The inhibition percentage was calculated using eq 3

$$I(\%) = \left(\frac{\text{Abs}_c - \text{Abs}_s}{\text{Abs}_C}\right) \times 100 \quad (3)$$

Abs_C is the absorbance of the study control and Abs_S is the test sample's absorbance. The concentration corresponding to 50% inhibition (IC_{50}) was calculated from the plot of the inhibition percentage against the extract concentration.

5.10. Preparation of the Spore Suspension for Antifungal Evaluation. Ten strains of toxigenic fungi, namely *A. flavus* ITEM 698, *A. parasiticus* ITEM 11, *A. carbonarius* ITEM 5010, *Aspergillus ochraceus* ITEM 5117, *Aspergillus oryzae* ITEM B5, *P. verrucosum* NRRL 695, *P. chrysogenum* ATCC 48271, *F. graminearum* ATCC 56091, *F. moniliforme* ITEM 52539, and *F. oxysporum* ITEM 12591, were utilized for the antifungal to determine the impact of oil and its microfluidized solution for fungal growth inhibition; also, two of them were used for the antiaflatoxigenic efficiency. These strains were gifted from the Food Toxicology and Contaminant Department, National Research Centre, Cairo, Egypt. The spore suspension was prepared using toxigenic fungal cultures cultivated on Czapek-Dox slant agar (22 + 1 °C/5 days). A sterile solution of Tween 80 (0.01%; v/v) was poured over the culture slant agar to obtain a conidial suspension. The slant surface was then gently scraped using a loop to aid the spores' release. The ultimate inoculum concentration ranged from 1.22 to 1.41 × 103 colony-forming units per milliliter (CFU/mL), as determined by using a Burker-Turk counting chamber (hemocytometer).

5.11. Determination of ASHEO and MF-ASHEO Activity against Toxigenic Fungi. The spore suspension of each fungus was spread on Czapek-Dox agar plates, where plate wells were loaded using 100 μL of crude or microfluidized essential oil.[10] The inhibition impact regarding the crude or microfluidized oil was recorded as an apparent zone diameter measured in millimeters for each fungus. The more the antifungal effect for each extract, the more the inhibition zone diameter. An antifungal standard material (fluconazole) was utilized as the control. Minimal antifungal concentration (MFC) was evaluated according to the method described by Badr et al.[60] Antifungal susceptibility was characterized using the broth microdilution method as per the Clinical Laboratory Standards Institute (CLSI)-approved standard M38-A2 guidelines suggested for toxigenic fungal strains under the investigation. The fluconazole, a standard fungicide, was applied as a control in this study.

5.12. Determination of Antimycotoxigenic Efficacy Using a Simulated Experiment. In the subsequent inquiry, two strains, *A. parasiticus* ITEM 11 and *P. verrucosum* NRRL 695, were chosen for further examination. The strains were seen to undergo reactivation on yeast extract sucrose (YES) medium during the acclimation phase. The concentrations of *A. parasiticus* (1.31×10^6) and *P. verrucosum* (1.96×10^5) were determined following sequential procedures. It is worth noting that these particular strains are recognized for their ability to create aflatoxins and ochratoxin A, respectively. The experimental procedure was implemented following Boudechicha et al.[8]-outlined methodology. Concisely, 5 mL of a spore suspension for each fungus was introduced separately into 250 mL of YES medium inside conical flasks. Following the incubation period, which lasted for 12 days/28 ± 2 °C, the media were filtered using Whatman No.1 filters. It is important to note that each filter had a predetermined weight. The filters that were gathered were subjected to a drying process in a hot air oven at a temperature of 45 °C for 16 h until a consistent weight was achieved for each filter. The calculation of mycelial weight loss was performed by using eq 4

$$\text{mycelial reduction (\%)} = [1 - (W_1 - W_2)] \times 100 \quad (4)$$

W_1: weight of the control dry mycelia and W_2: weight of the treated dry mycelia.

5.13. Evaluation of Mycotoxin Reduction in Simulated Media. Utilizing the filtered media resulting from the preceding stage, aflatoxins (AFs) were extracted and estimated in the growth medium of *A. parasiticus* media, and ochratoxin A (OCA) was assessed in *P. verrucosum* media. According to the previous methodology,[8] targeted mycotoxin concentrations were determined using a precalibrated fluorometer (VICAM Series 4EX fluorometer, Watertown, MA; LOD: 1.0 ng/L).

5.14. Molecular Docking. Enzyme crystal structures (isoleucyl-tRNA synthetase, DNA gyrase, dihydropteroate synthase, D-alanine: D-alanine ligase, IV topoisomerase, dihydrofolate reductase, and penicillin-binding protein 1a) were obtained from Protein DataBank (https://www.rcsb.org/, accessed on August 17, 2022) with the following PDB IDs: 1JZQ, 1KZN, 2VEG, 2ZDQ, 3RAE, 3SRW, and 3UDI. Aflatoxin biosynthesis enzymes (polyketide synthase: A0A1R3RGK0, nonribosomal peptide synthase: A0A1R3RGK1, cytochrome P450 monooxygenase: A0A1R3RGJ7, and halogenase: A0A1R3RGJ2) were acquired from UniProt (accessed on February 3, 2022). Carvacrol was downloaded from PubChem (accessed on May 3, 2023, *via* http://pubchem.ncbi.nlm.nih.gov/). The receptors were prepared by removing water and cocrystallized ligands/ions and protonated using Pymol software ver. 2.5.1. Ligands' 3D structures were optimized using Avogadro Software ver. 1.2.0. CB-DOCK2 performed blind docking (accessed on May 3, 2023, *via* http://clab.labshare.cn/cb-dock/php/).[65] The top five cavities were submitted to AutoDock Vina for docking. Best-docked complexes are analyzed using Discovery Studio software (ver. 21.1.0.20298), as described by Farouk et al.[66]

https://doi.org/10.1021/acsomega.4c00315
ACS Omega 2024, 9, 27030−27046

5.15. *In Silico* ADME Study. Carvacrol was evaluated for *in silico* ADME profiles using the SwissADME server (http://www.swissadme.ch/) from the Swiss Institute of Bioinformatics.[67] The SMILES notations were generated and submitted during the ligand preparation.

5.16. Statistical Analysis. All of the tests were undertaken in triplicate. The collected information is displayed as the mean value and standard deviation (SD). Data analyses were performed using GraphPad Prism 5 software (GraphPad Software Inc., La Jolla).

■ ASSOCIATED CONTENT

Supporting Information

The Supporting Information is available free of charge at https://pubs.acs.org/doi/10.1021/acsomega.4c00315.

Detailed GC-MS data in the oil and nanoemulsion (PDF)

■ AUTHOR INFORMATION

Corresponding Author

Amr Farouk − *Flavor and Aroma Chemistry Department, National Research Center, Cairo 12622, Egypt;* orcid.org/0000-0002-5261-2397; Email: af.mansour@nrc.sci.eg

Authors

Amel Boudechicha − *Laboratory of Applied Microbiology, Faculty of Natural and Life Sciences, University of Ferhat Abbas Setif1, Setif 19000, Algeria*

Abdelhakim Aouf − *Laboratory of Applied Microbiology, Faculty of Natural and Life Sciences, University of Ferhat Abbas Setif1, Setif 19000, Algeria*

Hatem Ali − *Food Technology Department, National Research Center, Cairo 12622, Egypt*

Tawfiq Alsulami − *Food Science & Nutrition Department, College of Food and Agricultural Sciences, King Saud University, Riyadh 11451, Saudi Arabia*

Ahmed Noah Badr − *Food Toxicology and Contaminants Department, National Research Centre, Cairo 12622, Egypt*

Zhaojun Ban − *Zhejiang Provincial Key Laboratory of Chemical and Biological Processing Technology of Farm Products; School of Biological and Chemical Engineering, Zhejiang University of Science and Technology, Hangzhou 310023, China*

Complete contact information is available at: https://pubs.acs.org/10.1021/acsomega.4c00315

Notes

The authors declare no competing financial interest.

■ ACKNOWLEDGMENTS

The authors thank the Researchers Supporting Project number (RSPD2024R641), King Saud University, Riyadh, Saudi Arabia, for funding this research. Thanks also to our late colleague, Dr. Lina Abed, who passed away in October 2023, for her technical assistance. We will all sorely miss Lina's outgoing personality and boundless talents.

■ REFERENCES

(1) Raut, J. S.; Karuppayil, S. M. A status review on the medicinal properties of essential oils. *Ind. Crops Prod.* **2014**, *62*, 250−264.

(2) Hamidpour, R.; Hamidpour, S.; Hamidpour, M.; Shahlari, M.; Sohraby, M. Summer Savory: From the Selection of Traditional Applications to the Novel Effect in Relief, Prevention, and Treatment of a Number of Serious Illnesses such as Diabetes, Cardiovascular Disease, Alzheimer's Disease, and Cancer. *J. Tradit. Complementary Med.* **2014**, *4*, 140−144.

(3) Nikolić, M.; Jovanović, K. K.; Marković, T.; Marković, D.; Gligorijević, N.; Radulović, S.; Soković, M. Chemical composition, antimicrobial, and cytotoxic properties of five *Lamiaceae* essential oils. *Ind. Crops Prod.* **2014**, *61*, 225−232.

(4) Chambre, D. R.; Moisa, C.; Lupitu, A.; Copolovici, L.; Pop, G.; Copolovici, D.-M. Chemical composition, antioxidant capacity, and thermal behavior of *Satureja hortensis* essential oil. *Sci. Rep.* **2020**, *10*, No. 21322.

(5) Katar, D.; Kacar, O.; Kara, N.; Aytaç, Z.; Göksu, E.; Kara, S.; Katar, N.; Erbaş, S.; Telci, I.; Elmastaş, M. Ecological variation of yield and aroma components of summer savory (*Satureja hortensis* L.). *J. Appl. Res. Med. Aromat. Plants* **2017**, *7*, 131−135.

(6) Djenane, D.; Aboudaou, M.; Ferhat, M. A.; Ouelhadj, A.; Ariño, A. Effect of the aromatisation with summer savory (*Satureja hortensis* L.) essential oil on the oxidative and microbial stabilities of liquid whole eggs during storage. *J. Essent. Oil Res.* **2019**, *31*, 444−455.

(7) Chouitah, O.; Meddah, B.; Sonnet, P. Chemical Composition and Antimicrobial Activity OF Essential Oil from the Leaves of *Satureja hortensis* L. *Alger. J. Nat. Prod.* **2018**, *6*, 639−644.

(8) Boudechicha, A.; Aouf, A.; Farouk, A.; Ali, H. S.; Elkhadragy, M. F.; Yehia, H. M.; Badr, A. N. Microfluidizing Technique Application for Algerian *Cymbopogon citratus* (DC.) Stapf Effects Enhanced Volatile Content, Antimicrobial, and Anti-Mycotoxigenic Properties. *Molecules* **2023**, *28*, No. 5367, DOI: 10.3390/molecules28145367.

(9) Fierascu, I.; Dinu-Pirvu, C. E.; Fierascu, R. C.; Velescu, B. S.; Anuta, V.; Ortan, A.; Jinga, V. Phytochemical Profile and Biological Activities of *Satureja hortensis* L.: A Review of the Last Decade. *Molecules* **2018**, *23*, No. 2458, DOI: 10.3390/molecules23102458.

(10) Razzaghi-Abyaneh, M.; Shams-Ghahfarokhi, M.; Yoshinari, T.; Rezaee, M. B.; Jaimand, K.; Nagasawa, H.; Sakuda, S. Inhibitory effects of *Satureja hortensis* L. essential oil on growth and aflatoxin production by *Aspergillus parasiticus*. *Int. J. Food Microbiol.* **2008**, *123*, 228−233.

(11) Mohtashami, S.; Rowshan, V.; Tabrizi, L.; Babalar, M.; Ghani, A. Summer savory (*Satureja hortensis* L.) essential oil constituent oscillation at different storage conditions. *Ind. Crops Prod.* **2018**, *111*, 226−231.

(12) Sabry, O. M. M.; El Sayed, A. M.; Alshalmani, S. K. GC/MS Analysis and Potential Cytotoxic Activity of *Haplophyllum tuberculatum* Essential Oils Against Lung and Liver Cancer Cells. *Pharmacogn. J.* **2015**, *8*, 66−69.

(13) Djenane, D.; Yangüela, J.; Amrouche, T.; Boubrit, S.; Boussad, N.; Roncalés, P. Chemical composition and antimicrobial effects of essential oils of *Eucalyptus globulus*, *Myrtus communis* and *Satureja hortensis* against *Escherichia coli* O157:H7 and *Staphylococcus aureus* in minced beef. *Food Sci. Technol. Int.* **2011**, *17*, 505−515.

(14) Mihajilov-Krstev, T.; Radnović, D.; Kitić, D.; Zlatković, B.; Ristić, M.; Branković, S. (2009). Chemical composition and antimicrobial activity of *Satureja hortensis* L. essential oil. *Open Life Sci.* **2009**, *4*, 411−416.

(15) Tozlu, E.; Cakir, A.; Kordali, S.; Tozlu, G.; Ozer, H.; Akcin, T. A. Chemical compositions and insecticidal effects of essential oils isolated from *Achillea gypsicola*, *Satureja hortensis*, *Origanum acutidens* and *Hypericum scabrum* against broadbean weevil (*Bruchus dentipes*). *Sci. Hortic.* **2011**, *130*, 9−17.

(16) Kizil, S.; Turk, M.; Özguven, M.; Khawar, K. M. Full Blooming Stage is Suitable for Herbage Yield and Essential Oil Content of Summer Savory (*Satureja hortensis* L.). *J. Essent. Oil Bear. Plants* **2009**, *12*, 620−629.

(17) Giweli, A.; Džamić, A. M.; Soković, M.; Ristić, M. S.; Marin, P. D. Antimicrobial and Antioxidant Activities of Essential Oils of *Satureja thymbra* Growing Wild in Libya. *Molecules* **2012**, *17*, 4836−4850, DOI: 10.3390/molecules17054836.

(18) Baher, Z. F.; Mirza, M.; Ghorbanli, M.; Rezaii, M. B. The influence of water stress on plant height, herbal and essential oil yield

and composition in *Satureja hortensis* L. *Flavour Fragrance J.* **2002**, *17*, 275−277.
(19) Aouf, A.; Ali, H.; Al-Khalifa, A. R.; Mahmoud, K. F.; Farouk, A. Influence of Nanoencapsulation Using High-Pressure Homogenization on the Volatile Constituents and Anticancer and Antioxidant Activities of Algerian *Saccocalyx satureioides* Coss. et Durieu. *Molecules* **2020**, *25*, No. 4756, DOI: 10.3390/molecules25204756.
(20) Salvia-Trujillo, L.; Rojas-Graü, M. A.; Soliva-Fortuny, R.; Martín-Belloso, O. Formulation of Antimicrobial Edible Nanoemulsions with Pseudo-Ternary Phase Experimental Design. *Food Bioprocess Technol.* **2014**, *7*, 3022−3032.
(21) Donsì, F.; Annunziata, M.; Sessa, M.; Ferrari, G. Nanoencapsulation of essential oils to enhance their antimicrobial activity in foods. *LWT–Food Sci. Technol.* **2011**, *44*, 1908−1914.
(22) Karsli, G. T.; Sahin, S.; Oztop, M. H. High-Pressure-Homogenized Clove and Thyme Oil Emulsions: Formulation, Stability, and Antioxidant Capacity. *ACS Food Sci. Technol.* **2022**, *2*, 1832−1839.
(23) Santamaría, E.; Maestro, A.; Vilchez, S.; González, C. Study of nanoemulsions using carvacrol/MCT-(Oleic acid-potassium oleate)/Tween 80 ®- water system by low energy method. *Heliyon* **2023**, *9*, No. e16967.
(24) Deng, L. L.; Taxipalati, M.; Que, F.; Zhang, H. Physical characterization and antioxidant activity of thymol solubilized Tween 80 micelles. *Sci. Rep.* **2016**, *6*, No. 38160.
(25) Salvia-Trujillo, L.; Rojas-Graü, A.; Soliva-Fortuny, R.; Martín-Belloso, O. Physicochemical characterization and antimicrobial activity of food-grade emulsions and nanoemulsions incorporating essential oils. *Food Hydrocolloids* **2015**, *43*, 547−556.
(26) McClements, D. J.; Rao, J. Food-Grade Nanoemulsions: Formulation, Fabrication, Properties, Performance, Biological Fate, and Potential Toxicity. *Crit. Rev. Food Sci. Nutr.* **2011**, *51*, 285−330.
(27) Arancibia, C.; Navarro-Lisboa, R.; Zúñiga, R. N.; Matiacevich, S. Application of CMC as Thickener on Nanoemulsions Based on Olive Oil: Physical Properties and Stability. *Int. J. Polym. Sci.* **2016**, *2016*, No. 6280581.
(28) Guerra-Rosas, M. I.; Morales-Castro, J.; Ochoa-Martínez, L. A.; Salvia-Trujillo, L.; Martín-Belloso, O. Long-term stability of food-grade nanoemulsions from high methoxyl pectin containing essential oils. *Food Hydrocolloids* **2016**, *52*, 438−446.
(29) Klang, V.; Matsko, N. B.; Valenta, C.; Hofer, F. Electron microscopy of nanoemulsions: an essential tool for characterization and stability assessment. *Micron* **2012**, *43*, 85−103.
(30) Popovici, R. A.; Vaduva, D.; Pinzaru, I.; Dehelean, C. A.; Farcas, C. G.; Coricovac, D.; Danciu, C.; Popescu, I.; Alexa, E.; Lazureanu, V.; Stanca, H. T. A comparative study on the biological activity of essential oil and total hydro-alcoholic extract of *Satureja hortensis* L. *Exp. Ther. Med.* **2019**, *18*, 932−942.
(31) Ding, H. M.; Ma, Y. Q. Theoretical and computational investigations of nanoparticle-biomembrane interactions in cellular delivery. *Small* **2015**, *11*, 1055−1071. 2015
(32) Milhomem-Paixão, S. S. R.; Fascineli, M. L.; Muehlmann, L. A.; Melo, K. M.; Salgado, H. L. C.; Joanitti, G. A.; Pieczarka, J. C.; Azevedo, R. B.; Santos, A. S.; Grisolia, C. K. Andiroba Oil (*Carapa guianensis* Aublet) Nanoemulsions: Development and Assessment of Cytotoxicity, Genotoxicity, and Hematotoxicity. *J. Nanomater* **2017**, *2017*, No. 4362046, DOI: 10.1155/2017/4362046.
(33) da Silva Gündel, S.; Velho, M. C.; Diefenthaler, M. K.; Favarin, F. R.; Copetti, P. M.; de Oliveira Fogaça, A.; Klein, B.; Wagner, R.; Gündel, A.; Sagrillo, M. R.; Ourique, A. F. Basil oil-nanoemulsions: Development, cytotoxicity and evaluation of antioxidant and antimicrobial potential. *J. Drug Delivery Sci. Technol.* **2018**, *46*, 378−383.
(34) Chime, S. A.; Kenechukwu, F. C.; Attama, A. A. Nanoemulsions — Advances in Formulation, Characterization and Applications in Drug Delivery. In *Application of Nanotechnology in Drug Delivery*; IntechOpen Limited, 2014.
(35) Watanabe, A.; Tanaka, H.; Sakurai, Y.; Tange, K.; Nakai, Y.; Ohkawara, T.; Takeda, H.; Harashima, H.; Akita, H. Effect of particle size on their accumulation in an inflammatory lesion in a dextran sulfate sodium (DSS)-induced colitis model. *Int. J. Pharm.* **2016**, *509*, 118−122.
(36) Baker, D. H. A.; Al-Moghazy, M.; ElSayed, A. A. A. The in vitro cytotoxicity, antioxidant and antibacterial potential of *Satureja hortensis* L. essential oil cultivated in Egypt. *Bioorg. Chem.* **2020**, *95*, No. 103559.
(37) Friedman, M. Chemistry and Multibeneficial Bioactivities of Carvacrol (4-Isopropyl-2-methylphenol), a Component of Essential Oils Produced by Aromatic Plants and Spices. *J. Agric. Food Chem.* **2014**, *62*, 7652−7670.
(38) Ćavar, S.; Maksimović, M.; Šolić, M. E.; Jerković-Mujkić, A.; Bešta, R. Chemical composition and antioxidant and antimicrobial activity of two Satureja essential oils. *Food Chem.* **2008**, *111*, 648−653.
(39) Khoury, M.; Stien, D.; Eparvier, V.; Ouaini, N.; El Beyrouthy, M. Report on the Medicinal Use of Eleven Lamiaceae Species in Lebanon and Rationalization of Their Antimicrobial Potential by Examination of the Chemical Composition and Antimicrobial Activity of Their Essential Oils. *Evidence-Based Complementary Altern. Med.* **2016**, *2016*, No. 2547169.
(40) Sharma, A. D.; Farmaha, M.; Kaur, I. Preparation and characterization of O/W nanoemulsion with eucalyptus essential oil and study of in vitro antibacterial activity. *J. Nanomed. Res.* **2020**, *5*, 347−354.
(41) Özogul, Y.; Özogul, F.; Kulawik, P. The antimicrobial effect of grapefruit peel essential oil and its nanoemulsion on fish spoilage bacteria and food-borne pathogens. *LWT* **2021**, *136*, No. 110362.
(42) Van Houdt, R.; Michiels, C. W. Biofilm formation and the food industry, a focus on the bacterial outer surface. *J. Appl. Microbiol.* **2010**, *109*, 1117−1131.
(43) Miladi, H.; Mili, D.; Slama, R. B.; Zouari, S.; Ammar, E.; Bakhrouf, A. Antibiofilm formation and anti-adhesive property of three Mediterranean essential oils against a foodborne pathogen Salmonella strain. *Microb. Pathog.* **2016**, *93*, 22−31.
(44) Sharifi, A.; Mohammadzadeh, A.; Salehi, T. Z.; Mahmoodi, P. Antibacterial, antibiofilm and antiquorum sensing effects of *Thymus daenensis* and *Satureja hortensis* essential oils against *Staphylococcus aureus* isolates. *J. Appl. Microbiol.* **2018**, *124*, 379−388.
(45) Martignago, C. C. S.; Soares-Silva, B.; Parisi, J. R.; e Silva, L. C. S.; Granito, R. N.; Ribeiro, A. M.; Renno, A. C. M.; de Sousa, L. R. F.; Aguiar, A. C. C. Terpenes extracted from marine sponges with antioxidant activity: a systematic review. *Nat. Prod. Bioprospect.* **2023**, *13*, No. 23, DOI: 10.1007/s13659-023-00387-y.
(46) Djordjevic, N.; Mancic, S.; Karabegovic, I.; Cvetkovic, D.; Stanojevic, J.; Savic, D.; Danilovic, B. Influence of the Isolation Method to the Composition and Antimicrobial and Antioxidative Activity of Winter Savory (*Satureja montana* L.) Essential Oil. *J. Essent. Oil Bear. Plants* **2021**, *24*, 386−399.
(47) Borges, R. S.; Keita, H.; Ortiz, B. L. S.; dos Santos Sampaio, T. I.; Ferreira, I. M.; Lima, E. S.; de Jesus Amazonas da Silva, M.; Fernandes, C. P.; de Faria Mota Oliveira, A. E. M.; da Conceição, E. C.; Rodrigues, A. B. L.; Filho, A. C. M. P.; Castro, A. N.; Carvalho, J. C. T. Anti-inflammatory activity of nanoemulsions of essential oil from *Rosmarinus officinalis* L.: in vitro and in zebrafish studies. *Inflammopharmacology* **2018**, *26*, 1057−1080.
(48) Ha, T. V. A.; Kim, S.; Choi, Y.; Kwak, H. S.; Lee, S. J.; Wen, J.; Oey, I.; Ko, S. Antioxidant activity and bioaccessibility of size-different nanoemulsions for lycopene-enriched tomato extract. *Food Chem.* **2015**, *178*, 115−121.
(49) Thompson, D. P. Inhibition of growth of mycotoxigenic Fusarium species by butylated hydroxyanisole and/or carvacrol. *J. Food Prot.* **1996**, *59*, 412−415.
(50) Jesus, F. P. K.; Ferreiro, L.; Bizzi, K. S.; Loreto, É.S.; Pilotto, M. B.; Ludwig, A.; Alves, S. H.; Zanette, R. A.; Santurio, J. M. In vitro activity of carvacrol and thymol combined with antifungals or antibacterials against *Pythium insidiosum*. *J. Mycol. Méd.* **2015**, *25*, e89−e93.

https://doi.org/10.1021/acsomega.4c00315
ACS Omega 2024, 9, 27030−27046

(51) Moon, H.; Rhee, M. S. Synergism between carvacrol or thymol increases the antimicrobial efficacy of soy sauce with no sensory impact. *Int. J. Food Microbiol.* **2016**, *217*, 35−41.
(52) Hajibonabi, A.; Yekani, M.; Sharifi, S.; Nahad, J. S.; Dizaj, S. M.; Memar, M. Y. Antimicrobial activity of nanoformulations of carvacrol and thymol: new trend and applications. *OpenNano* **2023**, *13*, No. 100170.
(53) de Freitas, R. F.; Schapira, M. A. Systematic analysis of atomic protein−ligand interactions in the PDB. *MedChemComm* **2017**, *8*, 1970−1981, DOI: 10.1039/c7md00381a.
(54) Brandl, M.; Weiss, M. S.; Jabs, A.; Sühnel, J.; Hilgenfeld, R. C-H···pi-interactions in proteins. *J. Mol. Biol.* **2001**, *307*, 357−377.
(55) El Abdali, Y.; Mahraz, A. M.; Beniaich, G.; Mssillou, I.; Chebaibi, M.; Jardan, Y. A. B.; Lahkimi, A.; Nafidi, H.-A.; Aboul-Soud, M. A. M.; Bourhia, M.; Bouia, A. Essential oils of Origanum compactum Benth: Chemical characterization, in vitro, in silico, antioxidant, and antibacterial activities. *Open Chem.* **2023**, *21*, No. 20220282.
(56) Khan, I.; Bahuguna, A.; Shukla, S.; Aziz, F.; Chauhan, A. K.; Ansari, M. B.; Bajpai, V. K.; Huh, Y. S.; Kang, S. C. Antimicrobial potential of the food-grade additive carvacrol against uropathogenic *E. coli* based on membrane depolarization, reactive oxygen species generation, and molecular docking analysis. *Microb. Pathog.* **2020**, *142*, No. 104046.
(57) Herrera-Calderon, O.; Yepes-Pérez, A. F.; Quintero-Saumeth, J.; Rojas-Armas, J. P.; Palomino-Pacheco, M.; Ortiz-Sánchez, J. M.; Cieza-Macedo, E. C.; Arroyo-Acevedo, J. L.; Figueroa-Salvador, L.; Peña-Rojas, G.; Andía-Ayme, V. Carvacrol: An In Silico Approach of a Candidate Drug on HER2, PI3Kα, mTOR, hER-α, PR, and EGFR Receptors in the Breast Cancer. *Evidence-Based Complementary Altern. Med.* **2020**, *2020*, No. 8830665.
(58) Salvia-Trujillo, L.; Rojas-Graü, M. A.; Soliva-Fortuny, R.; Martín-Belloso, O. Effect of processing parameters on physicochemical characteristics of microfluidized lemongrass essential oil-alginate nanoemulsions. *Food Hydrocolloids* **2013**, *30*, 401−407.
(59) Adams, R. P. *Identification of Essential Oil Components by Gas Chromatography/Mass Spectrometry*, 5th ed.; Texensis Publishing: Nashville, TN, USA, 2017.
(60) Badr, A. N.; El-Attar, M. M.; Ali, H. S.; Elkhadragy, M. F.; Yehia, H. M.; Farouk, A. Spent Coffee Grounds Valorization as Bioactive Phenolic Source Acquired Antifungal, Anti-Mycotoxigenic, and Anti-Cytotoxic Activities. *Toxins* **2022**, *14*, No. 109, DOI: 10.3390/toxins14020109.
(61) Santos, J. D. C.; Coelho, E.; Silva, R.; Passos, C. P.; Teixeira, P.; Henriques, I.; Coimbra, M. A. Chemical composition and antimicrobial activity of Satureja montana byproducts essential oils. *Ind. Crops Prod.* **2019**, *137*, 541−548.
(62) CLSI. *Methods for Dilution Antimicrobial Susceptibility Tests for Bacteria that Grow Aerobically*, 11th ed.; Clinical Laboratory Standards Institute: Wayne, PA, 2018.
(63) Stepanović, S.; Vukovic, D.; Dakic, I.; Savic, B.; Svabic-Vlahovic, M. A modified microtiter-plate test for quantification of staphylococcal biofilm formation. *J. Microbiol. Methods* **2000**, *40*, 175−179.
(64) Hatano, T.; Kagawa, H.; Yasuhara, T.; Okuda, T. Two new flavonoids and other constituents in licorice root: Their relative astringency and radical scavenging effects. *Chem. Pharm. Bull.* **1988**, *36*, 2090−2097.
(65) Liu, Y.; Yang, X.; Gan, J.; Chen, S.; Xiao, Z.-X.; Cao, Y. CB-Dock2: Improved protein−ligand blind docking by integrating cavity detection, docking and homologous template fitting. *Nucleic Acids Res.* **2022**, *50*, 159−164.
(66) Farouk, A.; Alsulami, T.; Ali, H. S.; Badr, A. N. In-Vitro and In-Silico Investigation for the Spent-Coffee Bioactive Phenolics as a Promising Aflatoxins Production Inhibitor. *Toxins* **2023**, *15*, No. 225, DOI: 10.3390/toxins15030225.
(67) Daina, A.; Michielin, O.; Zoete, V. SwissADME: a free web tool to evaluate pharmacokinetics, drug-likeness and medicinal chemistry friendliness of small molecules. *Sci. Rep.* **2017**, *7*, No. 42717, DOI: 10.1038/srep42717.

https://doi.org/10.1021/acsomega.4c00315
ACS Omega 2024, 9, 27030−27046